DFIG Active Damping Control Strategy Based on Remodeling of Multiple Energy Branches

Jing Ma, *Senior Member, IEEE*, and Yaqi Shen

***Abstract*—Concerning subsynchronous oscillation caused by the integration of doubly-fed induction generator (DFIG) to power grid via series compensation line, an active damping control strategy based on remodeling of multiple energy branches in DFIG is proposed. First, according to the flow path of oscillation components, energy branches in DFIG are divided. Second, potential energy and dissipation energy are defined characterizing accumulation and consumption of energy during oscillation. Then, by analyzing the contribution of energy branches to potential energy and dissipation energy, key energy branches affecting the stability of system are screened. On this basis, the relations among stator voltage, potential energy, and dissipation energy are established, and frequency-dependent energy compensation functions in key branches are derived. By assessing their impact on low voltage ride through (LVRT) performance of DFIG, the compensation branch compatible with DFIG fundamental frequency characteristics are screened. Then, take sub/supersynchronous frequency stability coefficient ratio as the objective function, and the requirement on stability in sub/supersynchronous frequency band as the constraints. The compensation branch parameter optimization scheme is established. Finally, a test system is built in RT-LAB for verification. Simulation results demonstrate that, the proposed strategy can realize active damping control in multiple oscillation cases, and guarantee the stability of system in full frequency band. Besides, the strategy does not affect LVRT performance of DFIG and is well compatible with DFIG fundamental frequency characteristics.**

***Index Terms*—Active damping control, dissipation energy, energy branches, potential energy, sub/supersynchronous oscillation.**

I. Introduction

In RECENT years, as the penetration rate of wind generation ever increases, subsynchronous oscillation occurs ever more frequently when doubly-fed wind farm is transmitted via the series compensation system. Consequently, trip-off of wind farms from grid frequently occurs, greatly endangering the safe and stable operation of power grid [1]–[4]. Therefore, how to effectively suppress subsynchronous oscillation in doubly-fed induction generator (DFIG) integrated power system and improve the stable operation ability of DFIG has become an urgent issue.

Currently, measures taken to suppress subsynchronous oscillation in DFIG-integrated power system can be categorized into two types, i.e., passive suppression measures and active suppression measures. Passive suppression measures mainly aim to improve the integration of wind turbine to grid, including adding reactive power compensation controller [5], [6] and switch ON/OFF control of series compensation line [7]. However, such suppression measures cannot solve subsynchronous oscillation problems from the source. Meanwhile, as the transmission capacity of wind turbine increases, the capacity of external control devices needed also increases, and the switching of series compensation line will be more frequent, which will increase the suppression cost and worsen the power quality. Existing active suppression measures mainly aim to improve the dynamic characteristic of wind turbine in sub/supersynchronous frequency band, including oscillation filtering, parameter optimization, and control system reconfiguration. Oscillation filtering method adds band-pass filter to the control link to filter oscillation components in control link and eliminate the coupling effect between generator and grid in subsynchronous frequency band [8]. However, parameters of such filter are set for certain fixed resonance frequency, thus, oscillation filtering method is only applicable to single oscillation case, and when the operation mode of power grid varies, such control strategy cannot adapt to the variation of oscillation frequency. Parameter optimization method quantifies the relationship between control parameters of wind turbine and system damping level and constructs control parameter optimization model to improve the stability of subsynchronous oscillation [9], [10]. However, due to the requirement on stable operation of wind turbine, the adjustable range of converter control parameters is limited. Control system reconfiguration method is a widely used control strategy, most of which increases the equivalent damping of DFIG RSC by adding control branch or link to converters [11]–[13]. However, the contribution of GSC to DFIG subsynchronous oscillation is neglected and most of the method also concern oscillation suppression at certain fixed resonance frequency, which are not applicable to multiple oscillation cases. Besides, there is no theoretical analysis of the impact of additional control link on fundamental frequency characteristics of wind turbine such

Manuscript received 14 April 2020; revised 29 June 2020, 21 August 2020, and 16 September 2020; accepted 17 September 2020. Date of publication 21 September 2020; date of current version 20 November 2020. This work was supported in part by the National Key Research and Development Program of China under Grant 2018YFB0904003, and in part by the Chinese Universities Scientific Fund under Grants 2018JQ01and 2018ZD01. Recommended for publication by Associate Editor M. Harfman Todorovic. *(Corresponding author: Jing Ma.)*

The authors are with the State Key Laboratory of Alternate Electrical Power System with Renewable Energy Sources, North China Electric Power University, Beijing 102206, China (e-mail: hdmajing@163.com; jsntsyq1994@163.com).

Color versions of one or more figures in this article are available at https://doi.org/10.1109/TPEL.2020.3025716.

Digital Object Identifier 10.1109/TPEL.2020.3025716

as LVRT, etc. Based on the abovementioned analysis, existing control strategies are limited to active suppression at certain fixed oscillation frequency. When the oscillation frequency varies in different oscillation cases, existing methods cannot meet the damping demand. Meanwhile, most of existing control strategies aim to improve the stability of wind turbine in subsynchronous frequency band, and few has taken supersynchronous frequency band and fundamental frequency band into consideration.

In view of the abovementioned problems, a DFIG active damping control strategy based on remodeling of multiple energy branches in RSC and GSC is proposed. The strategy conducts coordinated energy compensation in RSC and GSC energy channels based on the flow path of stator voltage perturbation in DFIG converter. It can realize active damping control with adaptability to different oscillation cases, compatibility with supersynchronous frequency band and DFIG fundamental frequency characteristics.

The rest of this article is organized as follows. In Section I, energy branches in RSC and GSC of DFIG are categorized. In Section II, the key energy branches that affect system potential energy and dissipation energy are screened. In Section III, energy compensation branches are designed in key energy branches of GSC and RSC, considering their compatibility with DFIG fundamental frequency characteristics and system stability in supersynchronous frequency band. In Section IV, RT-Lab hardware-in-the-loop simulation platform is built to verify the effectiveness of the proposed control strategy followed by the simulation results in Section V. Finally, Section VI concludes the article.

II. Model of DFIG-Integrated Power System

A. DFIG Energy Model

According to [14], DFIG dynamic energy can be expressed with electrical variables at the terminal of DFIG as

$$\Delta W_{\mathbf{DFIG}} = -\int \left(\Delta i_d d\Delta u_q - \Delta i_q d\Delta u_d\right) - \int \Delta P_e d\Delta\theta \tag{1}$$

where $\Delta W_{\mathbf{DFIG}}$ is DFIG dynamic energy. i_d, i_q, u_d, and u_q are, respectively, the d- and q-axis components of DFIG terminal current and voltage. P_e is DFIG terminal active power. θ is the angular difference between dq coordinate system and xy coordinate system. Δ represents the variation from steady-state value.

In (1), the current, voltage, and power at the terminal of DFIG can be expressed with the sum of stator-side component and grid-side component, thus, DFIG dynamic energy can be rewritten as

$$\begin{aligned}\Delta W_{\mathbf{DFIG}} =& -\int \left(\Delta i_{sd} d\Delta u_q - \Delta i_{sq} d\Delta u_d\right) - \int \Delta P_e d\Delta\theta \\ &- \int \left(\Delta i_{gd} d\Delta u_q - \Delta i_{gq} d\Delta u_d\right) - \int \Delta P_e d\Delta\theta \\ =& \Delta W_e + \Delta W_g\end{aligned} \tag{2}$$

where *s and g*, respectively, represent the stator-side and grid-side electrical variables.

It can be seen from (2) that, DFIG dynamic energy is composed of two energy parts, which are defined in this article as excitation energy ΔW_e and grid-side energy ΔW_g, which correspond to two energy channels in DFIG, as shown in Fig. 1. By further analyzing the detailed expressions of dynamic energy in the excitation channel and grid-side channel, the detailed DFIG dynamic energy model can be constructed.

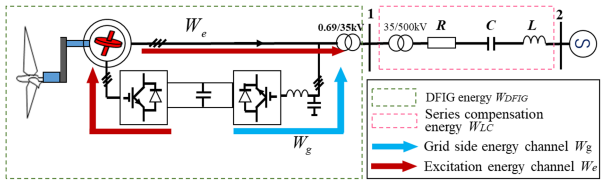

Fig. 1. Structure of DFIG and energy branches in DFIG.

1) Excitation Channel Energy

In DFIG excitation channel dynamic energy ΔW_e, the variation of DFIG terminal voltage is composed of two parts, i.e., the variation of voltage generated by the oscillation component in induction generator and the variation of rotor voltage generated by the oscillation component through rotor converter. Therefore, excitation channel dynamic energy ΔW_e can be expressed as the sum of induction generator energy and rotor converter energy, as shown in

$$\begin{aligned}\Delta W_{\mathrm{e}} &= \Delta W_{ig} + \Delta W_{r\_c} \\ &= -\int \left(\Delta i_{sd} d\Delta u_{q\_ig} - \Delta i_{sq} d\Delta u_{d\_ig}\right) - \int \Delta P_{e\_ig} d\Delta\theta \\ &\quad - \int \left(\Delta i_{sd} d\Delta u_{rq} - \Delta i_{sq} d\Delta u_{rd}\right) - \int \Delta P_{er} d\Delta\theta\end{aligned} \tag{3}$$

where ΔW_{ig} is induction generator energy, and ΔW_{r_c} is rotor converter energy. Δi_{rd} and Δi_{rq} are, respectively, the d-axis and q-axis components of rotor current. Δu_{rd} and Δu_{rq} are the variation of d- and q-axis components of the voltage generated by rotor converter, respectively. Δu_{d_ig} and Δu_{q_ig} are the variation of d-axis and q-axis components of the voltage generated by induction generator flux.

It can be seen from (3), the variation of excitation channel energy contains two parts, i.e., energy generated by the control effect of rotor converter, and energy generated by the flux of induction generator.

Expressions of two energy parts are analyzed as follows.

1) Energy Generated by the Induction Generator: DFIG applies stator flux directional control. Suppose stator flux is constant and stator resistance is neglected, according to generator flux equation, d-axis and q-axis components of the variation of rotor voltage and current can be obtained, shown in

$$\begin{cases}\Delta u_{d\_ig} = R_r \Delta i_{rd} - a_2\left(\omega_s - \omega_r\right)\Delta i_{rq} + a_2 \Delta \dot{i}_{rd} \\ \Delta u_{q\_ig} = R_r \Delta i_{rq} + a_2\left(\omega_s - \omega_r\right)\Delta i_{rd} + a_2 \Delta \dot{i}_{rq}\end{cases}$$

$$\begin{cases}\Delta i_{rd} = -\Delta i_{sd}/a_1 \\ \Delta i_{rq} = -\Delta i_{sq}/a_1\end{cases} \tag{4}$$

where ω_s is the synchronous speed, ω_r is rotor speed, and $a_1 = -L_m/L_s$ and $a_2 = L_r - {L_m}^2/L_s$, where L_s, L_r, and L_m are

the equivalent stator inductance, rotor inductance, and mutual inductance in *dq* coordinate system. R_r is rotor resistance. These parameters can be obtained by the parameter identification of the DFIG generator [15].

Apply (4) to the ΔW_{ig} in (3), so that the dynamic energy generated by induction generator during oscillation can be obtained

$$W_{ig} = -(\omega_r - \omega_d) R_r \int \Delta i^2 dt - (-\omega_r L_r/a_1 + \omega_r L_m) \times \int (\omega_r - \omega_d) \Delta i_{rd} \Delta i_{rq} dt \tag{5}$$

where $\omega_d = \omega_s - \omega_n$ is the oscillation frequency of system in *dq* coordinate system.

2) Energy Generated by the Control Link of Rotor Converter: According to the control structure of rotor converter, its output voltage can be expressed as

$$\begin{cases} \Delta u_{rd} = K_{p1}K_{p3}\Delta P_s + K_{i1}K_{p3}\int \Delta P_s dt - K_{p3}\Delta i_{rd} \\ + \int K_{p1}K_{i3}\Delta P_s dt + K_{i1}K_{i3}\iint \Delta P_s dtdt - K_{i3}\int \Delta i_{rd} dt \\ \Delta u_{rq} = K_{p2}K_{p3}\Delta Q_s + K_{i2}K_{p3}\int \Delta Q_s dt - K_{p3}\Delta i_{rq} \\ + \int K_{p2}K_{i3}\Delta Q_s dt + K_{i2}K_{i3}\iint \Delta Q_s dtdt - K_{i3}\int \Delta i_{rq} dt \end{cases} \tag{6}$$

where K_{p1} and K_{i1} are PI parameters of active power outer loop. K_{p2} and K_{i2} are PI parameters of reactive power outer loop. K_{p3} and K_{i3} are PI parameters of current inner loop. The PI parameters of the converter control system can be obtained by parameter identification methods in [16] and [17]. Considering the parameter identification is not the focus of this article, and thus it will not be explored in this article.

The variation of active power ΔP_s and reactive power ΔQ_s in (6) can be expressed as

$$\begin{cases} \Delta P_s = \Delta u_{sd}\Delta i_{sd} + \Delta u_{sq}\Delta i_{sq} + U_{sd0}\Delta i_{sd} + I_{sd0}\Delta u_{sd} \\ \Delta Q_s = \Delta u_{sq}\Delta i_{sd} + \Delta u_{sd}\Delta i_{sq} - U_{sd0}\Delta i_{sq} + I_{sd0}\Delta u_{sq} \end{cases} \tag{7}$$

where U_{sd0} and I_{sd0} are the initial values of stator *d*-axis voltage and current, respectively. They can be obtained by measuring the *d*-axis and *q*-axis components of rotor/stator voltage and current when DFIG is in steady-state operation.

The angular difference between *dq* and *xy* coordinate system $\Delta\theta$ is mainly affected by PLL control parameters. According to three-phase synchronous phase-locked control structure, the expression of $\Delta\theta$ can be obtained

$$\Delta\theta = -\int k_{p\theta}\Delta u_{sq} dt - \iint k_{i\theta}\Delta u_{sq} dtdt \tag{8}$$

where Δu_{sd} and Δu_{sq} are, respectively, the *d*- and *q*-axis components of the variation of stator voltage. They are caused by the perturbation components of voltage and current generated by the integration of series compensation line, where *C* compensation is considered to be applied. Their expressions can be written as

$$\begin{cases} \Delta u_{sd} = R\Delta i_{sd} + \omega_d L\Delta \dot{i}_{sd} - \omega_s L\Delta i_{sq} \\ \qquad -(\omega_d - \omega_s)^{-1}C^{-1}\Delta i_{sq} \\ \Delta u_{sq} = R\Delta i_{sq} - \omega_d L\Delta \dot{i}_{sq} + \omega_s L\Delta i_{sd} \\ \qquad +(\omega_d - \omega_s)^{-1}C^{-1}\Delta i_{sd} \end{cases} \tag{9}$$

where *R* is the equivalent resistance of transmission line. *L* is the reactance of power grid, which equals to the sum of transformer equivalent reactance and transmission line equivalent reactance. *C* is the series compensation capacitance. Its value is only determined by power grid dispatch center according to the demand on wind power transmission distance. When *C* is adjusted by power grid dispatch center, the series compensation degree $K = (\omega^2 LC)^{-1}$ varies and the oscillation scene excited by the coupling between DFIG and series compensation line also changes accordingly [10], [18]. As a result, in this article, *R*, *L*, and *C* are all inherent parameters of transmission line, reflecting system oscillation scene, respectively. The parameters will not be changed by the proposed control.

It should be noted that, (9) is not limited in C compensation. When *LC* compensation is applied, Δu_{sd} and Δu_{sq} can still be expressed as (9), but the definition of *L* must include the series compensation reactance in this case.

Apply (6)–(8) to the expression of ΔW_{r_c} in (3), so that the energy generated by rotor converter can be obtained

$$\Delta W_{c\_r} = \Delta W_{r\_i} + \Delta W_{r\_u} + \Delta W_{ui} + \Delta W_{\mathrm{PLL}} + \Delta W_{Lr}$$

$$\begin{cases} \Delta W_{r\_i} = \int \Delta i_{rd} d\left[-K_{p2}K_{p3}U_{sd0}\Delta i_{sq} - (K_{i2}K_{p3} + K_{p2}K_{i3})\int U_{sd0}\Delta i_{sq} dt - K_{i2}K_{i3}\iint U_{sd0}\Delta i_{sq} dtdt\right] \\ \quad - \int \Delta i_{rq} d\left[K_{p1}K_{p3}U_{sd0}\Delta i_{sd} + (K_{i1}K_{p3} + K_{p1}K_{i3}) \times \int U_{sd0}\Delta i_{sd} dt + K_{i1}K_{i3}\iint U_{sd0}\Delta i_{sd} dtdt\right] \\ \Delta W_{r\_u} = \int \Delta i_{rd} d\left[K_{p2}K_{p3}I_{sd0}\Delta u_{sq} + (K_{i2}K_{p3} + K_{p2}K_{i3})\int I_{sd0}\Delta u_{sq} dt + K_{i2}K_{i3}\iint I_{sd0}\Delta u_{sq} dtdt\right] \\ \quad - \int \Delta i_{rq} d\left[K_{p1}K_{p3}I_{sd0}\Delta u_{sq} + (K_{i1}K_{p3} + K_{p1}K_{i3}) \times \int I_{sd0}\Delta u_{sq} dt + K_{i1}K_{i3}\iint I_{sd0}\Delta u_{sq} dtdt\right] \\ \Delta W_{ui} = -\int \Delta i_{rd} d\left[-K_{p2}K_{p3}(\Delta u_{sq}\Delta i_{sd} + \Delta u_{sd}\Delta i_{sq}) - (K_{i2}K_{p3} + K_{p2}K_{i3})\int (\Delta u_{sq}\Delta i_{sd} + \Delta u_{sd}\Delta i_{sq}) dt\right] \\ \quad + \int \Delta i_{rd} d\left[K_{i2}K_{i3}\iint (\Delta u_{sq}\Delta i_{sd} + \Delta u_{sd}\Delta i_{sq}) dtdt\right] \\ \quad - \int \Delta i_{rq} d\left[K_{p1}K_{p3}(\Delta u_{sd}\Delta i_{sd} + \Delta u_{sq}\Delta i_{sq}) + (K_{i1}K_{p3} + K_{p1}K_{i3})\int (\Delta u_{sd}\Delta i_{sd} + \Delta u_{sq}\Delta i_{sq}) dt\right] \\ \quad - \int \Delta i_{rq} d\left[K_{i1}K_{i3}\iint (\Delta u_{sd}\Delta i_{sd} + \Delta u_{sq}\Delta i_{sq}) dtdt\right] \\ \Delta W_{\mathrm{PLL}} = \int U_{sd0}\Delta u_{sd}\left(K_{p\theta}\Delta u_{sq} - \int K_{i\theta}\Delta u_{sq} dt\right) dt \\ \quad - \int I_{sd0}\Delta u_{sd}\left(K_{p\theta}\Delta u_{sq} - \int K_{i\theta}\Delta u_{sq} dt\right) dt \\ \Delta W_{Lr} = 0.5 a_1^{-2}\omega_2 L_r \Delta i_s^2. \end{cases} \tag{10}$$

According to (10), the energy generated by rotor converter contains five components. ΔW_{r_i} is the dynamic energy component generated by stator current through rotor-side power outer loop and current inner loop, denoted as the excitation current energy branch. ΔW_{r_u} is the dynamic energy component generated by stator voltage through rotor-side power outer loop and current inner loop, denoted as the excitation voltage energy branch. ΔW_{iu} is the periodic energy component generated by the coupling between stator voltage and current, denoted as coupling energy. Since the periodic energy does not affect the variation trend of system overall energy, according to Lyapunov's stability theorem, it does not affect the stability of system. Thus, this energy component is not analyzed in detail. ΔW_{PLL} is the dynamic energy generated by PLL. ΔW_{Lr} is the

dynamic energy component generated by rotor reactance. ΔW_{Lr} and ΔW_{ig} jointly form the induction generator energy branch.

Furthermore, apply (9) to (10), and express all the stator voltage components in ΔW_{r_i} with stator current components, so that the detailed expressions of ΔW_{r_i}, ΔW_{r_u}, $\Delta W_{\rm PLL}$, and ΔW_{ig} in the excitation channel can be obtained

$$\begin{aligned}
\Delta W_{r_i} =& -\frac{1}{a_1}K_{p3}\int \omega_d \Delta i_s^2 dt + \frac{1}{a_1}\frac{1}{\omega_d}\int K_{i2}K_{i3}U_{sd0}\Delta i_{sd}^2 dt \\
&+ \frac{1}{a_1}\frac{1}{\omega_d}\int K_{i1}K_{i3}U_{sd0}\Delta i_{sq}^2 dt - \int \frac{1}{a_1}K_{p2}K_{p3}U_{sd0}\Delta i_{sd}^2 dt \\
&- \int \frac{1}{a_1}K_{p1}K_{p3}U_{sd0}\Delta i_{sq}^2 dt \\
\Delta W_{r_u} =& \frac{1}{a_1}K_{i1}K_{p3}I_{sd0}\int \left[(\omega_d-\omega_s)L - \frac{1}{\omega_d-\omega_s}\frac{1}{C}\right] \\
&\times \Delta i_{sq}^2 dt + \frac{1}{a_1}\int K_{p1}K_{p3}I_{sd0}\omega_d R\Delta i_{sq}^2 dt \\
&- \frac{1}{a_1}\int K_{i1}K_{i3}I_{sd0}R\frac{1}{\omega_d}\Delta i_{sq}^2 dt + \frac{1}{a_1}K_{p1}K_{i3}I_{sd0} \\
&\times \int \left[(\omega_d-\omega_s)L - \frac{1}{\omega_d-\omega_s}\frac{1}{C}\right]\Delta i_{sq}^2 dt + \frac{1}{a_1}K_{p1}K_{p3}I_{sd0}\frac{1}{2} \\
&\times \left[(\omega_d-\omega_s)L - \frac{1}{\omega_d-\omega_s}\frac{1}{C}\right]\Delta i_{sq}^2 + \frac{1}{a_1}K_{i2}K_{p3}I_{sd0} \\
&\times \int \left[(\omega_d-\omega_s)L - \frac{1}{\omega_d-\omega_s}\frac{1}{C}\right]\Delta i_{sd}^2 dt - \frac{1}{a_1} \\
&\times \int K_{p2}K_{p3}I_{sd0}\omega_d R\Delta i_{sd}^2 dt - \frac{1}{a_1}\int K_{i2}K_{i3}I_{sd0}R\frac{1}{\omega_d}\Delta i_{sd}^2 dt \\
&+ \frac{1}{a_1}K_{p2}K_{i3}I_{sd0}\int \left[(\omega_d-\omega_s)L - \frac{1}{\omega_d-\omega_s}\frac{1}{C}\right]\Delta i_{sd}^2 dt \\
&+ \frac{1}{a_1}K_{p2}K_{p3}I_{sd0}\frac{1}{2}\left[(\omega_d-\omega_s)L - \frac{1}{\omega_d-\omega_s}\frac{1}{C}\right]\Delta i_{sd}^2 \\
\Delta W_{PLL} =& \int I_{sd0}\left\{K_{p\theta}R^2 - K_{p\theta}\left[(\omega_d-\omega_s)L\right.\right. \\
&\left.\left. - \frac{1}{\omega_d-\omega_s}\frac{1}{C}\right]\right\}\Delta i_{sq}\Delta i_{sd}dt + \int \frac{I_{sd0}}{\omega_d}\left\{K_{i\theta}R^2\Delta i_{sq}^2\right. \\
&\left. + K_{i\theta}\left[(\omega_d-\omega_s)L - \frac{1}{\omega_d-\omega_s}\frac{1}{C}\right]\Delta i_{sd}^2\right\}dt + \int U_{sd0} \\
&\times \left\{\frac{K_{i\theta}}{\omega_d}R + K_{p\theta}\left[(\omega_d-\omega_s)L - \frac{1}{\omega_d-\omega_s}\frac{1}{C}\right]\right\}\Delta i_{sq}\Delta i_{sd}dt \\
&- \int U_{sd0}\left\{K_{p\theta}R\Delta i_{sq}^2 + \frac{K_{i\theta}}{\omega_d}\left[(\omega_d-\omega_s)L\right.\right. \\
&\left.\left. - \frac{1}{\omega_d-\omega_s}\frac{1}{C}\right]\Delta i_{sd}^2\right\}dt \\
\Delta W_{Lr} =& 0.5a_1^{-2}\omega_2 L_r \Delta i_s^2. \qquad (11)
\end{aligned}$$

According to (11), the expressions of dynamic energy in excitation channel can be unified as energy with d-axis and q-axis components of stator current as the state variables. The terms in the aperiodic component of PLL dynamic energy $\Delta W_{\rm PLL}$ are all related with $1/\omega_d$. Since the value of ω_d is much larger than the values of converter parameters K_p and K_i, i.e., the values of the terms containing $1/\omega_d$ are very small, the dynamic energy generated by PLL is much smaller than the energy of the other three branches. Thus, DFIG excitation channel energy is mainly composed of three energy branches, i.e., excitation current energy branch, excitation voltage energy branch, and induction generator energy branch. It should be noted that, though the expression of ΔW_{r_u} in (11) is related with stator current component, this energy component is generated by the flow of stator voltage in rotor converter, and it still corresponds to the excitation voltage energy branch.

C. Grid-Side Channel Energy

According to the control structure of grid-side converter, its output voltage Δu_{dg} and Δu_{qg} can be expressed as

$$\begin{cases}
\Delta u_{gd} = -K_{p4}K_{p5}\Delta u_{dc} - \int K_{i4}K_{p5}\Delta u_{\rm dc}dt - K_{p5}\Delta i_{gd} \\
-\int K_{i5}K_{p4}\Delta u_{\rm dc}dt - \iint K_{i4}K_{i5}\Delta u_{\rm dc}dtdt - \int K_{i5}\Delta i_{gd}dt \\
\Delta u_{gq} = -K_{p5}\Delta i_{gq} - \int K_{i5}\Delta i_{gd}dt
\end{cases} \qquad (12)$$

where K_{p4} and K_{i4} are PI parameters of voltage outer loop. K_{p5} and K_{i5} are PI parameters of current inner loop. $\Delta u_{\rm dc}$ is dc bus voltage. Δi_{dg} and Δi_{qg} are, respectively, the d- and q-axis components of grid-side converter output current.

According to power balance equations on two sides of dc bus voltage, the expression of dc bus voltage $\Delta u_{\rm dc}$ in (12) can be obtained

$$\begin{aligned}
C_{\rm dc}U_{\rm dc}\Delta \dot{u}_{\rm dc} =& \Delta u_{gd}\Delta i_{gd} + U_{gd0}\Delta i_{gd} + I_{gd0}\Delta u_{gd} \\
&- \left(\Delta u_{rd}\Delta i_{rd} + U_{rd0}\Delta i_{rd} + I_{rd0}\Delta u_{rd}\right). \qquad (13)
\end{aligned}$$

Apply (12) and (13) to the ΔW_g in (3), so that the detailed expression of grid-side channel energy can obtained. Since the value of ω_d is much larger than the values of converter parameters K_{p4} and K_{p5}, i.e., the values of the terms containing $1/\omega_d$ are very small, the energy components that contain $1/\omega_d$ are neglected in this article. Thus, the expression of grid-side channel energy can be approximated to

$$\begin{aligned}
\Delta W_g =& \Delta W_{C_i} + \Delta W_{C_u} + \Delta W_{gi} + \Delta W_{Lg} + \Delta W_{g_ui} \\
\Delta W_{C_i} =& K_{p5}K_{p4}/C_{\rm dc}\int (-I_{rd0}K_{p1}K_{p3}I_{sd0}\omega_d a_3 \Delta i_{sq}^2 \\
&- I_{rd0}K_{p1}K_{p3}U_{sd0}a_3\omega_d\Delta i_{sq}^2)dt \\
\Delta W_{C_u} =& -\frac{K_{p5}K_{p4}}{C_{\rm dc}}I_{rd0}K_{p1}K_{p3}I_{sd0}a_3\frac{1}{2} \\
&\times \left[(\omega_d-\omega_s)L - \frac{1}{\omega_d-\omega_s}\frac{1}{C}\right]\Delta i_{gd}^2 \\
&- \frac{K_{p5}K_{p4}}{C_{dc}}\int (I_{rd0}a_3K_{i1}K_{p3} + I_{sd0}a_3K_{p1}K_{i3})
\end{aligned}$$

TABLE I
DFIG ENERGY COMPONENTS AND CORRESPONDING ENERGY BRANCHES

Energy components	Energy branches
ΔW_{r_i}	the excitation current energy branch
ΔW_{r_u}	the excitation current energy branch
ΔW_{Lr}+ΔW_{ig}	induction generator energy branch
ΔW_{c_i}	the grid-side outer-loop current energy branch
ΔW_{c_u}	the grid-side outer-loop voltage energy branch
ΔW_{gi}	the grid-side inner-loop current energy branch
ΔW_{Lg}	the grid-side filtering reactance energy branch

$$\times \Delta i_{sq}^2 \left[(\omega_d-\omega_s)L-\frac{1}{\omega_d-\omega_s}\frac{1}{C}\right]dt+\frac{K_{p5}K_{i4}}{C_{\rm dc}}$$
$$\times\int I_{rd0}K_{i1}K_{p3}I_{sd0}a_3\left[(\omega_d-\omega_s)L-\frac{1}{\omega_d-\omega_s}\frac{1}{C}\right]$$
$$\Delta i_{sq}^2dt+\frac{K_{p5}K_{p4}}{C_{dc}}\int I_{gd0}Ra_3\omega_d\Delta i_{sq}^2dt$$
$$\Delta W_{gi}=\int \omega_d K_{p5}\Delta i_g^2 dt$$
$$\Delta W_{Lg}=0.5\omega_g L_g\Delta i_g^2$$
$$\Delta W_{g\_ui}=-\int \Delta i_{gq}d\left[-K_{p4}K_{p5}\left(\Delta u_{gd}\Delta i_{gd}-\Delta u_{rd}\Delta i_{rd}\right)\right.$$
$$\left.-\int K_{i4}K_{p5}\left(\Delta u_{gd}\Delta i_{gd}-\Delta u_{rd}\Delta i_{rd}\right)dt\right]$$
$$-\int \Delta i_{gq}d\left[-\int K_{i5}K_{p4}\left(\Delta u_{gd}\Delta i_{gd}-\Delta u_{rd}\Delta i_{rd}\right)dt\right.$$
$$\left.-\iint K_{i4}K_{i5}\left(\Delta u_{gd}\Delta i_{gd}-\Delta u_{rd}\Delta i_{rd}\right)dtdt\right]. \quad (14)$$

It can be seen from (14) that grid-side channel energy contains four energy branches, where $\Delta W_{c\cdot r}$ is the dynamic energy component generated by the variation of dc bus voltage caused by the oscillation component of rotor current through grid-side voltage outer loop and *d*-axis current inner loop, denoted as the grid-side outer-loop current energy branch. $\Delta W_{c\cdot u}$ is the dynamic energy component generated by the variation of dc bus voltage caused by the oscillation component of rotor voltage through grid-side voltage outer loop and *d*-axis current inner loop, denoted as the grid-side outer-loop voltage energy branch. ΔW_{gi} is the dynamic energy component generated by the oscillation component of grid-side current through current inner-loop control, denoted as the grid-side inner-loop current energy branch. ΔW_{Lg} is the dynamic energy component generated by grid-side filtering reactance, denoted as the grid-side filtering reactance energy branch. $\Delta W_{g\cdot ui}$ is the periodic energy component generated by the coupling between grid-side voltage and current. Since the periodic energy does not affect the stability of system. Thus, this energy component is not analyzed in detail.

Based on the abovementioned analysis, there are totally seven energy branches in DFIG, and the characteristic of DFIG dynamic energy is determined by them. The energy components and the corresponding energy branches are shown in Table I. The impact of each energy branch on system oscillatory stability is analyzed as follows.

III. ANALYSIS OF ENERGY BRANCHES IN DFIG-INTEGRATED POWER SYSTEM

A. Energy Stability Criterion

According to (8) and (11), DFIG dynamic energy can be written as

$$\Delta W_{\rm DFIG}=\frac{1}{2}\xi(\omega)\Delta i_{dqs}^2-\int\eta(\omega)\Delta i_{dqs}^2dt+\int\varsigma_{mn}(\omega)\Delta i_{ds}^m\Delta i_{qs}^n dt \quad (15)$$

where $\xi(\omega)=\xi_{r\_u}(\omega)+\xi_{ig}(\omega)+\xi_{c\_u}(\omega)+\xi_{\rm Lg}(\omega)$, $\xi_{r\_u}(\omega)$, $\xi_{ig}(\omega)$, $\xi_{c\_u}(\omega)$, and $\xi_{\rm Lg}(\omega)$ are the potential energy coefficient of the excitation current energy branch, induction generator energy branch, the grid-side outer-loop voltage energy branch, and the grid-side filtering reactance energy branch, respectively. The expressions of these potential energy coefficients are shown as follows:

$$\begin{cases}\xi_{r\_u}(\omega)=a_1^{-1}K_{p1}K_{p3}I_{ds0}/2\\ \quad\times\left[(\omega_d-\omega_s)L-(\omega_d-\omega_s)^{-1}C^{-1}\right]\\ \quad+a_1^{-1}K_{p2}K_{p3}I_{ds0}/2\left[(\omega_d-\omega_s)L-(\omega_d-\omega_s)^{-1}C^{-1}\right]\\ \xi_{ig}(\omega)=0.5a_1^{-2}\omega_2L_r\\ \xi_{C\_u}(\omega)=-0.5K_{p5}K_{p4}I_{dr0}K_{p1}K_{p3}I_{ds0}a_3/C_{\rm dc}\\ \quad\times\left[(\omega_d-\omega_s)L-(\omega_d-\omega_s)^{-1}C^{-1}\right]\\ \xi_{Lg}(\omega)=0.5a_3^{-2}\omega_gL_g.\end{cases}$$

$\eta(\omega) = \eta_{r\_i}(\omega)+\eta_{r\_u}(\omega)+\eta_{ig}(\omega)+\eta_{c\_i}(\omega)+\eta_{c\_u}(\omega)+\eta_{gi}(\omega)$, $\eta_{r\_i}(\omega)$, $\eta_{r\_u}(\omega)$, $\eta_{ig}(\omega)$, $\eta_{c\_i}(\omega)$, $\eta_{c\_u}(\omega)$, and $\eta_{gi}(\omega)$ are, respectively, the dissipation coefficient of the excitation current energy branch, the excitation voltage energy branch, the induction generator energy branch, the grid-side outer-loop current energy branch, the grid-side outer-loop voltage energy branch, and the grid-side inner-loop current energy branch. The expressions of these dissipation energy coefficients are shown as follows:

$$\begin{cases}\eta_{r\_i}(\omega)=-a_1^{-1}K_{p3}\omega_d+a_1^{-1}\omega_d^{-1}K_{i2}K_{i3}U_{ds0}\\ +a_1^{-1}\omega_d^{-1}K_{i1}K_{i3}U_{ds0}-a_1^{-1}K_{p2}K_{p3}U_{ds0}\\ -a_1^{-1}K_{p1}K_{p3}U_{ds0}\\ \eta_{r\_u}(\omega)=a_1^{-1}K_{i1}K_{p3}I_{ds0}[(\omega_d-\omega_s)L-(\omega_d-\omega_s)^{-1}C^{-1}]\\ +a_1^{-1}K_{p1}K_{p3}I_{ds0}\omega_dR-a_1^{-1}\omega_d^{-1}K_{i1}K_{i3}I_{ds0}R\\ +a_1^{-1}K_{p1}K_{i3}I_{ds0}\left[(\omega_d-\omega_s)L-(\omega_d-\omega_s)^{-1}C^{-1}\right]\\ +a_1^{-1}K_{i2}K_{p3}I_{ds0}[(\omega_d-\omega_s)L-(\omega_d-\omega_s)^{-1}C^{-1}]\\ -a_1^{-1}K_{p2}K_{p3}I_{ds0}\omega_dR-a_1^{-1}K_{i2}K_{i3}I_{ds0}R\omega_d^{-1}\\ +a_1^{-1}K_{p2}K_{i3}I_{ds0}[(\omega_d-\omega_s)L-(\omega_d-\omega_s)^{-1}C^{-1}]\\ \eta_{ig}(\omega)=-(\omega_r-\omega_d)R_r\\ \eta_{C\_i}(\omega)=-K_{p5}K_{p4}/C_{\rm dc}(I_{dr0}K_{p1}K_{p3}I_{ds0}\omega_da_3\\ +I_{dr0}K_{p1}K_{p3}U_{ds0}a_3\omega_d)\\ \eta_{C\_u}(\omega)=-K_{p5}K_{p4}/C_{\rm dc}(I_{dr0}a_3K_{i1}K_{p3}+I_{ds0}a_3K_{p1}K_{i3})\\ \times\left[(\omega_d-\omega_s)L-(\omega_d-\omega_s)^{-1}C^{-1}\right]+K_{p5}K_{i4}/\\ C_{\rm dc}I_{dr0}K_{i1}K_{p3}I_{ds0}a_3\left[(\omega_d-\omega_s)L-(\omega_d-\omega_s)^{-1}C^{-1}\right]\\ +K_{p5}K_{p4}/C_{\rm dc}I_{dg0}Ra_3\omega_d\\ \eta_{gi}(\omega)=\omega_dK_{p5}.\end{cases}$$

$\zeta_{mn}(\omega)$ is the coefficient of the nonconservative energy term, which varies periodically. Since the periodic energy does not affect the variation trend of system overall energy, according to Lyapunov's stability theorem, it does not affect the stability of system. However, in order to show the relationship between (15) and the expression of each energy branch, the detailed expression of $\zeta_{mn}(\omega)$ is added as follows:

$$
\begin{cases}
\varsigma_{11}(\omega) = -a_1^{-2}\left(-\omega_r L_r/a_1 + \omega_r L_m\right)(\omega_r - \omega_d) \\
+I_{sd0}\{K_{p\theta}R^2 - K_{p\theta}[(\omega_d-\omega_s)L - (\omega_d-\omega_s)^{-1}C^{-1}]\} \\
+U_{sd0}\{K_{i\theta}\omega_d^{-1}R + K_{p\theta}[(\omega_d-\omega_s)L - (\omega_d-\omega_s)^{-1}C^{-1}]\} \\
\varsigma_{21}(\omega) = -a_1^{-1}K_{p2}K_{p3}\{-R\omega_d \\
-4\omega_d[(\omega_d-\omega_s)L - (\omega_d-\omega_s)^{-1}C^{-1}]\} - a_1^{-1}(K_{i2}K_{p3} \\
+K_{p2}K_{i3})\{2R - [(\omega_d-\omega_s)L - (\omega_d-\omega_s)^{-1}C^{-1}]\} \\
-a_1^{-1}K_{i2}K_{i3}(2\omega_d)^{-1}R - a_3^{-1}\left(K_{i4}K_{p5} + K_{i5}K_{p4}\right)R/C \\
-a_1^{-1}K_{i1}K_{i3}(2\omega_d)^{-1}[(\omega_d-\omega_s)L - (\omega_d-\omega_s)^{-1}C^{-1}] \\
+a_3^{-1}K_{i4}K_{i5}/C_{dc}(2\omega_d)^{-1}[(\omega_d-\omega_s)L - (\omega_d-\omega_s)^{-1}C^{-1}] \\
+a_1^{-1}a_3^{-1}\left(K_{i4}K_{p5} + K_{i5}K_{p4}\right)K_{p2}K_{p3}/C_{dc}(-2R\omega_d) \\
+a_1^{-1}a_3^{-1}\left(K_{i4}K_{p5} + K_{i5}K_{p4}\right)K_{i2}K_{p3}/ \\
C_{dc}[(\omega_d-\omega_s)L - (\omega_d-\omega_s)^{-1}C^{-1}] \\
+a_1^{-1}a_3^{-1}\left(K_{i4}K_{p5} + K_{i5}K_{p4}\right)K_{p2}K_{i3}/ \\
C_{dc}[(\omega_d-\omega_s)L - (\omega_d-\omega_s)^{-1}C^{-1}] \\
+a_1^{-1}a_3^{-1}\left(K_{i4}K_{p5} + K_{i5}K_{p4}\right)/C_{dc}K_{i2}K_{i3}(2\omega_d)^{-1}R \\
+a_1^{-1}a_3^{-1}K_{i4}K_{i5}/C_{dc}\left(K_{i1}K_{p3} + K_{p1}K_{i3}\right)\omega_d R \\
+a_1^{-1}\left(K_{i1}K_{p3} + K_{p1}K_{i3}\right)R + a_1^{-1}a_3^{-1}K_{i4}K_{i5}K_{i1}K_{i3}/ \\
C_{dc}[(\omega_d-\omega_s)L - (\omega_d-\omega_s)^{-1}C^{-1}] \\
\varsigma_{12}(\omega) = -a_1^{-1}K_{p2}K_{p3}R\omega_d + a_1^{-1}K_{i2}K_{i3}(2\omega_d)^{-1}R \\
-a_1^{-1}\left(K_{i2}K_{p3} + K_{p2}K_{i3}\right)[(\omega_d-\omega_s)L - (\omega_d-\omega_s)^{-1}C^{-1}] \\
-a_1^{-1}K_{i1}K_{i3}(2\omega_d)^{-1}[(\omega_d-\omega_s)L - (\omega_d-\omega_s)^{-1}C^{-1}] \\
-a_3^{-1}\left(K_{i4}K_{p5} + K_{i5}K_{p4}\right)R/ \\
C_{dc} + a_1^{-1}\left(K_{i1}K_{p3} + K_{p1}K_{i3}\right)R \\
+a_3^{-1}K_{i4}K_{i5}/C_{dc}(2\omega_d)^{-1}[(\omega_d-\omega_s)L - (\omega_d-\omega_s)^{-1}C^{-1}] \\
+a_3^{-1}a_1^{-1}K_{p4}K_{p5}/C_{dc}\left(K_{i1}K_{p3} + K_{p1}K_{i3}\right)R\omega_d \\
+a_3^{-1}a_1^{-1}K_{p4}K_{p5}K_{i1}K_{i3}[(\omega_d-\omega_s)L - (\omega_d-\omega_s)^{-1}C^{-1}] \\
+a_3^{-1}a_1^{-1}\left(K_{i4}K_{p5} + K_{i5}K_{p4}\right)/ \\
C_{dc}K_{i1}K_{p3}\omega_d[(\omega_d-\omega_s)L - (\omega_d-\omega_s)^{-1}C^{-1}] \\
+a_3^{-1}a_1^{-1}\left(K_{i4}K_{p5} + K_{i5}K_{p4}\right)/ \\
C_{dc}K_{p1}K_{i3}\omega_d[(\omega_d-\omega_s)L - (\omega_d-\omega_s)^{-1}C^{-1}] \\
+a_1^{-1}a_3^{-1}K_{i4}K_{i5}/C_{dc}\left(K_{i1}K_{p3} + K_{p1}K_{i3}\right)R \\
+a_1^{-1}a_3^{-1}K_{i4}K_{i5}K_{i1}K_{i3}/C_{dc}(2\omega_d)^{-1} \\
\times[(\omega_d-\omega_s)L - (\omega_d-\omega_s)^{-1}C^{-1}].
\end{cases}
$$

It can be seen from (15) that during oscillation, the dynamic energy of DFIG-integrated power system is composed of three parts. The first part is potential energy term, which only has to do with the initial values of state variables and represents the energy accumulated during oscillation. $\xi(\omega)$ is defined as potential energy coefficient, which reflects the ability of system to accumulate energy during oscillation. The second part is dissipation term related with the integration path, which represents the energy consumed during perturbation. $\eta(\omega)$ is defined as dissipation energy coefficient, which reflects the ability of system to dissipate the energy accumulated during oscillation. The third part is nonconservative term related with the integration path, which varies periodically and does not affect the damping level of system. Therefore, DFIG dynamic energy is mainly composed of potential energy and dissipation energy.

According to Lyapunov's second stability theorem, for a free dynamic system, if the variation rate of system overall energy $V(V > 0)$, i.e.,$\dot{V}(x)$ is constantly negative, system overall energy will keep decreasing until it reaches the minimum value, when the system will be stable in an equilibrium state. Thus, if the variation of DFIG dynamic energy $\Delta W_{\mathrm{DFIG}}(t)$ gradually decreases, i.e., if $\Delta W_{\mathrm{DFIG}}(t)|_t^{t+\Delta t} < 0$, system overall energy will keep decreasing to the minimum value, when the system reaches stable state. Select one oscillation period as the time interval, the stability criterion of DFIG-integrated power system is as follows:

$$\frac{1}{2}\xi(\omega)\Delta x_{dqs}^2\Big|_{t_1}^{t_1+T} < \int_{t_1}^{t_1+T}\eta(\omega)\Delta x_{dqs}^2 dt \tag{16}$$

where T is one oscillation period.

It can be seen from (16) that when the dissipation energy of system is larger than the potential energy of system accumulated during oscillation, system overall energy will gradually decrease, i.e., the system can completely dissipate the potential energy generated during oscillation, thus, system oscillation will gradually go stable. Otherwise, system overall energy will gradually increase, and system oscillation will finally go unstable. Therefore, the potential energy term and dissipation term are key factors that determine the stability of system. According to (15), both of the terms are, respectively, determined by potential energy coefficient and dissipation energy coefficient, and both vary as the oscillation frequency varies. Thus, the stability of system also differs in different frequency bands.

According to (16), system stability coefficient can be defined as

$$\mu(\omega) = \frac{\eta(\omega)}{\xi(\omega)}. \tag{17}$$

It can be seen from (17) that the bigger dissipation energy coefficient $\eta(\omega)$ is and the smaller potential energy coefficient $\xi(\omega)$ is, the higher system stability coefficient $\mu(\omega)$ is, the higher system stability level is in this frequency band. Therefore, by regulating potential energy coefficient and dissipation energy coefficient, the stability of system sub/supersynchronous oscillation can be improved. On one hand, by increasing the dissipation energy coefficient, the ability of system to dissipate the accumulated potential energy can be improved, thus, the converging of oscillation can be accelerated. On the other hand, by decreasing the potential energy coefficient, the potential energy that system needs to consume can be decreased, thus, the oscillation amplitude can be lowered for faster converging of oscillation.

Considering that dissipation energy coefficient and potential energy coefficient are jointly determined by multiple energy branches, the contribution degree of each energy branch to them

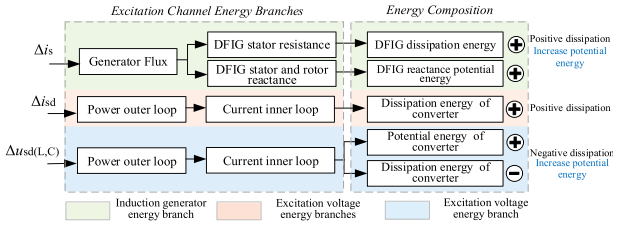

Fig. 2. Composition of excitation channel energy branches.

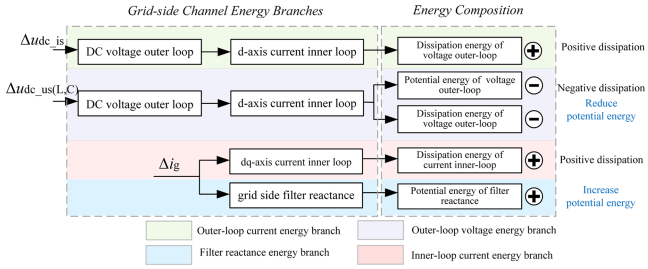

Fig. 3. Composition of grid-side channel energy branches.

need be studied further, so that the key energy branches that affect the stability of system can be discovered, and the location for potential energy and dissipation energy compensation can be determined.

B. Excitation Channel Energy Branches

According to (11), the composition of potential energy and dissipation energy in excitation channel energy branches is shown in Fig. 2.

In Fig. 2, the potential energy in DFIG excitation channel is jointly generated by induction generator energy branch and excitation voltage energy branch. However, since the value of generator rotor reactance is much smaller than that of line reactance, the potential energy in DFIG excitation channel is mainly affected by excitation voltage energy branch, and its energy coefficient is

$$\Delta\xi_{ur}(\omega) = \frac{1}{a_1}\left(K_{p1}K_{p3} + K_{p2}K_{p3}\right) I_{sd0} \times \left[\left(\omega_d - \omega_s\right) L - \frac{1}{\omega_d - \omega_s}\frac{1}{C}\right]. \tag{18}$$

It can be seen from (18) that the potential energy coefficient in excitation voltage energy branch is positive, i.e., during oscillation, the oscillation component of stator voltage will accumulate potential energy through excitation voltage energy branch. In this case, according to (17), system stability coefficient will drop, which makes against the converging of oscillation.

The dissipation energy in DFIG excitation channel is jointly generated by three energy branches. Since the value of generator rotor resistance is much smaller than the dissipation energy coefficients of excitation voltage and current energy branches, the dissipation energy in DFIG excitation channel is mainly affected by excitation voltage energy branch and excitation current energy branch. The dissipation energy coefficients of these two branches are

$$\begin{aligned}\Delta\eta_{ir}(\omega) = & -\frac{1}{a_1}K_{p3}\omega_d + \frac{1}{a_1}\frac{1}{\omega_d}K_{i2}K_{i3}U_{sd0} \\ & + \frac{1}{a_1}\frac{1}{\omega_d}K_{i1}K_{i3}U_{sd0} - \frac{1}{a_1}K_{p2}K_{p3}U_{sd0} - \frac{1}{a_1}K_{p1}K_{p3}U_{sd0} \\ \Delta\eta_{ur}(\omega) = & -\frac{1}{a_1}K_{i1}K_{p3}I_{sd0}\left[\left(\omega_d - \omega_s\right) L - \frac{1}{\omega_d - \omega_s}\frac{1}{C}\right] \\ & + \frac{1}{a_1}K_{p1}K_{p3}I_{sd0}\omega_d R - \frac{1}{a_1}K_{i1}K_{i3}I_{sd0}R\frac{1}{\omega_d} \\ & + \frac{1}{a_1}K_{p1}K_{i3}I_{sd0}\left[\left(\omega_d - \omega_s\right) L - \frac{1}{\omega_d - \omega_s}\frac{1}{C}\right] \\ & - \frac{1}{a_1}K_{i2}K_{p3}I_{sd0}\left[\left(\omega_d - \omega_s\right) L - \frac{1}{\omega_d - \omega_s}\frac{1}{C}\right] \\ & + \frac{1}{a_1}K_{p2}K_{p3}I_{sd0}\omega_d R - \frac{1}{a_1}K_{i2}K_{i3}I_{sd0}R\frac{1}{\omega_d} \\ & + \frac{1}{a_1}K_{p2}K_{i3}I_{sd0}\left[\left(\omega_d - \omega_s\right) L - \frac{1}{\omega_d - \omega_s}\frac{1}{C}\right].\end{aligned} \tag{19}$$

It can be seen from (19) that in excitation current energy branch, the terms containing K_i are all negative. However, since the value of ω_d is much larger than the values of PI control parameters, the terms containing ${\omega_d}^{-1}$ can all be neglected. Thus, the dissipation energy coefficient of excitation current energy branch is positive, i.e., it has positive contribution to system stability coefficient.

Besides, there is a negative term in the dissipation energy coefficient of excitation voltage energy branch. According to (17), it has negative contribution to system stability.

C. Grid-Side Channel Energy Branches

According to (14), the composition of potential energy and dissipation energy in grid-side channel energy branches is shown in Fig. 3.

It can be seen from Fig. 3 that the potential energy in grid-side energy channel is mainly generated by filtering reactance energy branch and voltage outer loop energy branch, and the corresponding potential energy coefficients are

$$\begin{aligned}\Delta\xi_{ug}(\omega) = & -\frac{K_{p5}K_{p4}}{C_{dc}}I_{rd0}K_{p1}K_{p3}I_{sd0}a_3\frac{1}{2} \times \left[\left(\omega_d - \omega_s\right) L - \frac{1}{\omega_d - \omega_s}\frac{1}{C}\right] \\ \Delta\xi_{LG}(\omega) = & \frac{1}{2}\omega_g L_g.\end{aligned} \tag{20}$$

According to (20), the potential energy term of voltage outer loop energy branch is negative, which is beneficial for the offset of positive potential energy accumulated during oscillation. Besides, since grid-side filtering reactance is much smaller than the potential energy coefficient of voltage outer loop energy branch, the potential energy generated by filtering reactance

energy branch can be neglected. Thus, there is no need for potential energy compensation in the abovementioned two energy branches.

The dissipation energy in grid-side energy channel is generated by grid-side outer-loop voltage and current energy branches and inner-loop current energy branch. Their corresponding dissipation energy coefficients are

$$\begin{aligned}\Delta\eta_{ig\_o}(\omega) &= \frac{K_{p5}K_{p4}}{C_{dc}}(-I_{rd0}K_{p1}K_{p3}I_{sd0}\omega_d a_3 \\ &\quad - I_{rd0}K_{p1}K_{p3}U_{sd0}a_3\omega_d) \\ \Delta\eta_{ug\_o}(\omega) &= -\frac{K_{p5}K_{p4}}{C_{dc}}(I_{rd0}a_3K_{i1}K_{p3} + I_{sd0}a_3K_{p1}K_{i3}) \\ &\quad \times \left[(\omega_d-\omega_s)L - \frac{1}{\omega_d-\omega_s}\frac{1}{C}\right] \\ &\quad + \frac{K_{p5}K_{i4}}{C_{dc}}I_{rd0}K_{i1}K_{p3}I_{sd0}a_3\left[(\omega_d-\omega_s)L\right. \\ &\quad \left. - \frac{1}{\omega_d-\omega_s}\frac{1}{C}\right] + \frac{K_{p5}K_{p4}}{C}I_{gd0}Ra_3\omega_d \\ \Delta\eta_{ug\_i}(\omega) &= \omega_d K_{p5}. \end{aligned} \tag{21}$$

It can be seen from (21) that the dissipation energy coefficients of grid-side outer-loop current energy branch and grid-side inner-loop current energy branch are both positive. However, in the former energy branch, there exists a negative dissipation term. Thus, it has negative contribution to system stability.

Based on the abovementioned analysis, excitation voltage energy branch is the key energy branch that affects the potential energy and dissipation energy in DFIG excitation channel; grid-side outer-loop voltage energy branch is the key energy branch that affects the dissipation energy in grid-side channel. By conducting potential energy and dissipation energy compensation in these two energy branches to increase system dissipation energy coefficient and lower potential energy coefficient, the stability of system can be improved, and fast suppression of subsynchronous oscillation can be realized.

Besides, according to (18)–(21), the potential energy term and dissipation term both contain parameters *R*, *L,* and *C,* which reflect the oscillation scene of grid-connected DFIG. The corresponding potential energy coefficient and dissipation energy coefficient both vary as the series compensation degree and oscillation frequency vary. In other words, when the series compensation degree of DFIG transmission line changes, the excited oscillation scene also changes, so does the energy compensation need of system. Therefore, compensation of potential energy and dissipation energy should adapt to different oscillation cases.

IV. Remodeling of Multiple Energy Branches and Active Damping Optimization Control

According to the abovementioned analysis, the oscillation component of stator voltage is the key factor that affects the coupling between DFIG and grid. The negative dissipation term and positive potential energy term caused by its flow in the key energy branches both vary with the oscillation frequency and series compensation degree. By introducing stator voltage compensation terms to the excitation channel and grid-side channel, energy compensation branches adaptive to the oscillation frequency can be constructed. Meanwhile, considering their impact on DFIG fundamental frequency characteristics and system stability in supersynchronous frequency band, the location and parameters of energy compensation branches can be optimized. Thus active damping control of DFIG in sub/supersynchronous frequency band can be realized. The overall design and operation procedure of control strategy is shown in Fig. 4.

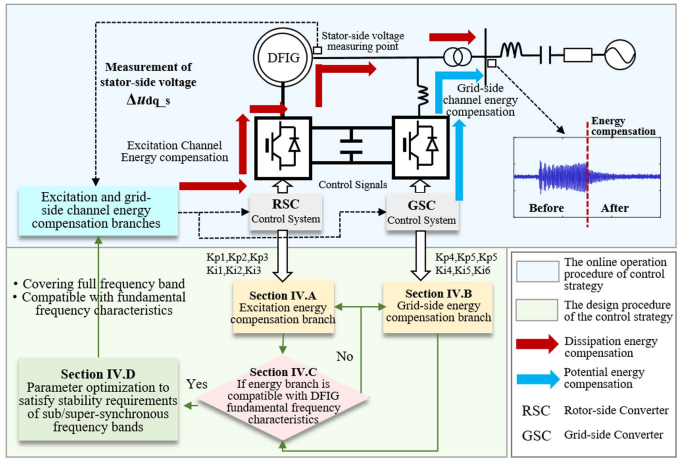

Fig. 4. Design and operation procedure of control strategy based on energy compensation branches.

The overall design procedure is shown in the green frame in Fig. 4. The design of the proposed control strategy mainly contains three parts, i.e., design of energy compensation branches, check of fundamental frequency characteristics and parameter optimization of energy compensation branches. The design of energy compensation branches refers to constructing dissipation energy and potential energy compensation branches in excitation channel and grid-side channel. The check of fundamental frequency characteristics refers to exploring how the introduction of energy compensation branches affects DFIG fundamental frequency characteristics, and screening out those compatible with the characteristics. Parameter optimization of energy compensation branches refers to optimizing the control parameters of energy compensation branches so that the stability requirements of both subsynchronous and supersynchronous frequency bands can be satisfied.

The online operation procedure of control strategy is shown in the blue frame in Fig. 4. The designed excitation voltage compensation branch and grid-side voltage compensation branch are introduced to DFIG rotor-side and grid-side converter control systems. When oscillation occurs, DFIG stator-side voltage measuring point will input the measured oscillation component of stator voltage to the energy compensation branches. Then, the dissipation energy compensation and potential energy compensation can be generated via converter control systems. Therefore, DFIG damping level can be improved, and system oscillation can be effectively suppressed.

Next, the design process of each part will be described in detail.

A. Remodeling of Excitation Channel Energy

Containing both positive potential energy terms and negative dissipation terms, excitation voltage energy branch is the key energy branch in excitation channel. Therefore, both potential energy compensation and dissipation energy compensation are needed for this energy branch.

1) Potential Energy Compensation for Excitation Voltage Energy Branch: Apply (9) to the expression of excitation voltage energy branch in (11), retaining the rotor current term in the integrand and replacing the integration variable stator current with stator voltage components, so that the relationship between stator voltage components and the potential energy of excitation voltage energy branch can be derived

$$\begin{aligned}\Delta W_{rp} &= \int \Delta \mathbf{i_{sdq}} \mathbf{K_n} \mathbf{P_{LC}}(\omega)\, d\Delta \mathbf{i_{sdq}^T} \\ &= \int \Delta \mathbf{i_{sdq}} \mathbf{K_n} \mathbf{P_{LC}}(\omega) d\mathbf{P_{LC}^{-T}}(\omega)\, \Delta \mathbf{u_{sdq}^T} \\ &= \int \Delta \mathbf{i_{rdq}} (-a_1 \mathbf{K_n}) \begin{bmatrix} 0 & 1 \\ -1 & 0 \end{bmatrix} d\Delta \mathbf{u_{sdq}^T} \end{aligned} \tag{22}$$

where

$$\boldsymbol{K_n} = \begin{bmatrix} K_{p1}K_{p3}I_{ds0} & 0 \\ 0 & K_{p2}K_{p3}I_{ds0} \end{bmatrix}$$

$$\boldsymbol{P_{LC}}(\omega) = \begin{bmatrix} 0 & (\omega_d - \omega_s)L \\ -(\omega_d - \omega_s)L & -(\omega_d - \omega_s)^{-1}C^{-1} \\ +(\omega_d - \omega_s)^{-1}C^{-1} & 0 \end{bmatrix}.$$

Comparison between the integration variables of (2) and (22) reveals that stator voltage components generate a proportional gain on rotor voltage after it passes rotor converter, thus affecting the potential energy coefficient of excitation voltage energy branch. Therefore, a potential energy compensation branch reverse to the proportional gain of stator voltage components can be added to excitation voltage energy branch. It can be expressed as

$$\begin{aligned}\Delta W_{add\_u} &= -\int \Delta \mathbf{i_{rdq}} \mathbf{K}_c \begin{bmatrix} 0 & 1 \\ -1 & 0 \end{bmatrix} d\Delta \mathbf{u_{sdq}^T} \\ &= -\frac{1}{a_1}\int \omega_d K_{pc1} R \Delta i_s^2 dt - \frac{1}{a_1} K_{pc1} \\ &\quad \times \left[(\omega_d - \omega_s) L - \frac{1}{\omega_d - \omega_s}\frac{1}{C} \right] \Delta i_s^2 \\ \Delta \xi_{cr\_p} &= -\frac{1}{2a_1} K_{pc1} \left[(\omega_d - \omega_s) L - \frac{1}{\omega_d - \omega_s}\frac{1}{C} \right] \\ \Delta \eta_{cr\_p} &= -\frac{1}{a_1}\omega_d K_{pc1} R \end{aligned} \tag{23}$$

where K_{pc1} is the control parameter of energy compensation branch.

The control structure of the added energy compensation branch is shown in red line in Fig. 5, where the high-pass filter is used to filter the steady-state dc component of rotor current.

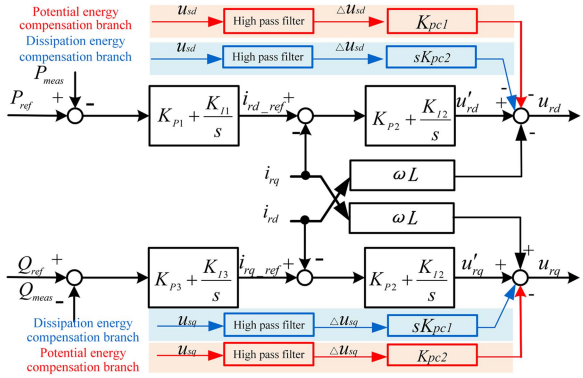

Fig. 5. Control structure of rotor converter.

It can be seen from (23) that the potential energy compensation term in the added energy compensation branch contains parameters L and C. The potential energy coefficient of it increases as the oscillation frequency and series compensation degree increase, thus, the energy compensation branch can effectively reduce the energy accumulated during oscillation and improve system stability in different oscillation cases.

Besides, according to (23), the added compensation branch generates positive dissipation compensation in subsynchronous frequency band and can improve system stability. However, affected byω_d, in supersynchronous frequency band, the coupled dissipation term may exhibit negative dissipation compensation and will to some degree decrease system stability coefficient in supersynchronous frequency band.

2) Dissipation Energy Compensation for Excitation Voltage Energy Branch: Apply (9) to the expression of excitation voltage energy branch in (11), retaining the rotor current term in the integrand and replacing the integration variable stator current with stator voltage components, so that the relationship between stator voltage components and the dissipation energy of excitation voltage energy branch can be derived

$$\begin{aligned}\Delta W_{rd} &= \int \Delta \mathbf{i_{sdq}} \mathbf{K}_d \frac{1}{\omega_d^2} \mathbf{P_{RLC}}(\omega)\, d\left(\Delta \mathbf{i'_{sdq}}\right)^T \\ &= \int \Delta \mathbf{i_{sdq}} \mathbf{K}_d \frac{1}{\omega_d^2} \mathbf{P_{RLC}}(\omega) d\mathbf{P_{RLC}^{-T}}(\omega) \left(\Delta \mathbf{u'_{sdq}}\right)^T \\ &= \int \Delta \mathbf{i_{rdq}} (-a_1 \mathbf{K}_d) \frac{1}{\omega_d^2} \begin{bmatrix} 0 & 1 \\ -1 & 0 \end{bmatrix} d\left(\Delta \mathbf{u'_{sdq}}\right)^T \end{aligned} \tag{24}$$

where $\mathbf{K}_d = \begin{bmatrix} K_{p1}K_{p3}I_{ds0} & K_{i1}K_{p3}I_{ds0} \\ K_{i2}K_{p3}I_{ds0} & K_{p2}K_{p3}I_{ds0} \end{bmatrix}$.

Comparison between the integration variables of (2) and (24) reveals that stator voltage components generate a differential gain on rotor voltage after it passes rotor converter, thus affecting the dissipation energy in excitation channel. According to (24), a dissipation energy compensation branch reverse to the differential gain of stator voltage components can be added to excitation voltage energy branch. Thus, system dissipation energy coefficient can be improved. The control structure of the added energy compensation branch is shown in blue line in Fig. 5. The added dissipation energy compensation branch can

be expressed as

$$\begin{aligned}\Delta W_{add\_ud} &= -\int \Delta \mathbf{i_{rdq}} \mathbf{K}_c \begin{bmatrix} 0 & 1 \\ -1 & 0 \end{bmatrix} d\left(\Delta \mathbf{u}'_{\mathbf{sdq}}\right)^T \\ &= \frac{1}{a_1}\int \omega_d^2 K_{pc2}\left[\left(\omega_d-\omega_s\right)L - \frac{1}{\omega_d-\omega_s}\frac{1}{C}\right] \\ &\quad \Delta i_s^2 dt + \frac{1}{a_1}\omega_d K_{pc2} R \Delta i_s^2 \\ \Delta \xi_{cr\_d} &= a_1^{-1}\omega_d K_{pc2} R \\ \Delta \eta_{cr\_d} &= \frac{1}{a_1}\omega_d^2 K_{pc2}\left[\left(\omega_d-\omega_s\right)L - \frac{1}{\omega_d-\omega_s}\frac{1}{C}\right]. \end{aligned} \quad (25)$$

It can be seen from (25) that this energy compensation branch will generate both dissipation energy compensation term and potential energy compensation term. The dissipation energy compensation term is constantly positive, and the corresponding dissipation coefficient increases as ω_d and series compensation degree increase. Thus, it exhibits positive dissipation compensation in both subsynchronous and supersynchronous frequency bands, and can effectively improve the stability of system. The potential energy coefficient of potential energy compensation term is negative, thus, it can reduce the energy accumulated during oscillation and improve system stability. However, in supersynchronous frequency band, this compensation term will provide positive potential energy compensation and increase the energy accumulated during oscillation.

B. Remodeling of Grid-Side Channel Energy

According to the abovementioned analysis, voltage outer-loop energy branch is the key energy branch that affects the dissipation energy in grid-side channel. Therefore, a dissipation energy compensation branch is added to it to realize remodeling of energy in the channel.

Apply (9) to the expression of voltage outer-loop energy branch in (14), so that the relationship between stator voltage components and the negative dissipation energy of voltage outer-loop energy branch can be derived, shown in (23)

$$\begin{aligned}\Delta W_{gd} &= \int \Delta \mathbf{i_{sd}} \mathbf{K}_{dg} \frac{1}{\omega_d^2}\mathbf{P_{LC}}(\omega)\, d\Delta \mathbf{i}'_{\mathbf{sd}} \\ &= \int \Delta \mathbf{i_{sd}} \mathbf{K}_{dg} \frac{1}{\omega_d^2}\mathbf{P_{LC}}(\omega) d\mathbf{P}_{\mathbf{LC}}^{-\mathbf{T}}(\omega)\, \Delta \mathbf{u}'_{\mathbf{sd}} \\ &= \int \Delta \mathbf{i_{gd}} \left(a_3 \mathbf{K}_{dg}\right) \frac{1}{\omega_d^2}\begin{bmatrix} 0 & 1 \\ -1 & 0 \end{bmatrix} d\Delta \mathbf{u}'_{\mathbf{sd}} \end{aligned} \quad (26)$$

where $\mathbf{K}_{dg} = -K_{p5}K_{p4}(I_{dr0}K_{i1}K_{p3} + I_{ds0}K_{p1}K_{i3})/C_{\mathrm{dc}}$.

Comparison between (2) and (26) reveals that, stator voltage components generate a differential gain on grid-side voltage after it passes grid-side converter, thus affecting the dissipation energy in grid-side channel. Therefore, a dissipation energy compensation branch reverse to the differential gain of stator voltage components can be added to grid-side channel, the control structure of which is shown in red line in Fig. 6.

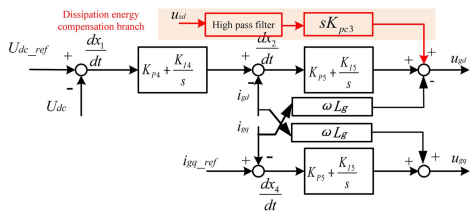

Fig. 6. Control structure of grid-side converter.

The added dissipation energy compensation branch can be expressed as

$$\begin{aligned}\Delta W_{add\_ug} &= -\int \Delta \mathbf{i}_{gq} \mathbf{K}_c \begin{bmatrix} 0 & 1 \\ -1 & 0 \end{bmatrix} d\Delta \mathbf{u}'_{\mathbf{sd}} \\ &= -\frac{1}{2a_3}\int \omega_d^2 K_{pc3}\left[\left(\omega_d-\omega_s\right)L - \frac{1}{\omega_d-\omega_s}\frac{1}{C}\right] \\ &\quad \Delta i_s^2 dt - \frac{1}{2a_3}\omega_d K_{pc3} R \Delta i_s^2 \\ \Delta \xi_{cr\_g} &= -\frac{1}{2a_3}\omega_d K_{pc3} R \\ \Delta \eta_{cr\_g} &= -\frac{1}{2a_3}\omega_d^2 K_{pc3}\left[\left(\omega_d-\omega_s\right)L - \frac{1}{\omega_d-\omega_s}\frac{1}{C}\right] \end{aligned} \quad (27)$$

where a_3 is the proportion coefficient between grid-side current and stator current $a_3 > 0$.

It can be seen from (27) that the dissipation energy compensation term in grid-side energy compensation branch can increase the dissipation coefficient in sub/supersynchronous frequency band, thus improving the stability of system in full frequency band. However, the potential energy compensation term in it exhibits different compensation effects in subsynchronous and supersynchronous frequency bands. In subsynchronous frequency band, the corresponding coefficient is negative, thus, the potential energy compensation term can reduce the potential energy accumulated during oscillation and improve system stability. However, in supersynchronous frequency band, the corresponding potential energy coefficient turns positive, thus, it may increase system potential energy and lower system stability. Consider that the value of ω_d is much larger than that of PI control parameters and line resistance, the dissipation energy compensation term is much larger than the potential energy compensation term. Therefore, generally the added energy compensation branch still exhibits dissipation energy compensation effect.

It should be noted that, in the expressions of excitation channel and grid-side channel compensation energy, *R*, *L*, and *C* are all inherent parameters reflecting system oscillation scene. It means the proposed energy compensation branches can adapt to different oscillation cases when providing compensation energy. But the proposed control strategy will not change the values of *R*, *L*, and *C*, and series compensation line itself does not participate in energy compensation. Meanwhile, whether C or *LC* compensation is applied in the transmission line, the effectiveness of the proposed method will not be influenced.

C. Verification of Fundamental Frequency Characteristics

The proposed energy compensation branches are mainly for the suppression of sub/supersynchronous oscillation in DFIG-integrated power system. However, the introduction of energy compensation branch strengthens the coupling between system perturbation and converter and may affect the dynamic characteristics of DFIG in nonsub/supersynchronous frequency band, which is called fundamental frequency characteristics in this article. Therefore, it is necessary to check their impact on fundamental frequency characteristics of DFIG.

According to guidelines for grid connection of wind power, DFIG should have low voltage ride through (LVRT) capability during short circuit fault [19], [20]. Therefore, the impact of energy compensation branches on LVRT performance of DFIG is analyzed in this article as an example. During LVRT, in order to guarantee normal operation of converter, the variation of rotor current should stay within a reasonable range [21]. Thus, by deriving the increment of rotor current generated by excitation channel energy compensation branch during short circuit fault, the compatibility of energy compensation branch with LVRT can be analyzed.

Combine (4), (23), and (25), so that the relationship between stator voltage and rotor current, after the energy compensation branch is introduced, can be obtained

$$\begin{cases} a_2\Delta\dot{i}_{rd\_c} + R_r\Delta i_{rd\_c} - \left(L_rL_s - L_m^2\right)\omega_2\Delta i_{rq\_c}/ \\ L_s = K_{pc1}\Delta u_{sd} + K_{pc2}\Delta\dot{u}_{sd} \\ a_2\Delta\dot{i}_{rq\_c} + R_r\Delta i_{rq\_c} + \left(L_rL_s - L_m^2\right)\omega_2\Delta i_{rd\_c}/ \\ L_s = K_{pc1}\Delta u_{sq} + K_{pc2}\Delta\dot{u}_{sq} \end{cases} \tag{28}$$

where Δi_{rd_c} and Δi_{rq_c} are, respectively, *d*-axis and *q*-axis components of the increment of rotor current generated by energy compensation branch.

After short circuit fault occurs, suppose *d*-axis and *q*-axis perturbation components of stator voltage are

$$\begin{cases} \Delta u_{sd} = U_0\cos\left(\omega_v t\right) \\ \Delta u_{sq} = -U_0\sin\left(\omega_v t\right) \end{cases} \tag{29}$$

where $\omega_v = \omega_s - \omega_p$. ω_p is the oscillation frequency of perturbation component, which is usually low frequency.

Apply (28) to (29), so that the *d*- and *q*-axis forced components of rotor current generated by energy compensation branch can be obtained

$$\begin{cases} \Delta i_{rd\_c} = A\cos\left(\omega_v t\right) + B\sin\left(\omega_v t\right) \\ \Delta i_{rq\_c} = \left(L_rL_s - L_m^2\right)\omega_2/ \\ \quad L_s\left(a_2B\omega_v + R_rA - K_cU_0\right)\cos\left(\omega_v t\right) \\ \quad + \left(L_rL_s - L_m^2\right)\omega_2/L_s\left(-a_2A\omega_v + R_rB\right)\sin\left(\omega_v t\right). \end{cases} \tag{30}$$

The expressions of coefficients *A* and *B* are

$$A = -\frac{\left[\left(a_2\omega_v - \left(L_rL_s - L_m^2\right)\omega_s/L_s\right)^2 + R_r^2\right]}{\left(R_r^2 + \left(L_rL_s - L_m^2\right)/L_s\omega_2 - a_2^2\omega_v^2\right)^2 + \left(2a_2R_r\omega_v\right)^2}K_{pc1}R_rU_0 + \frac{\left[\left(a_2\omega_v - \left(L_rL_s - L_m^2\right)\omega_s/L_s\right)^2 + R_r^2\right]}{\left(R_r^2 + \left(L_rL_s - L_m^2\right)/L_s\omega_2 - a_2^2\omega_v^2\right)^2 + \left(2a_2R_r\omega_v\right)^2} \times \left(K_{pc2}a_2\omega_v^2L_s/\left(L_rL_s - L_m^2\right) + K_{pc2}\omega_v\right)U_0$$

$$B = \frac{2a_2R_r^2\omega_v + \left(\left(L_rL_s - L_m^2\right)\omega_2/L_s - a_2\omega_v\right)^2 \times \left(\left(L_rL_s - L_m^2\right)\omega_2/L_s + a_2\omega_v\right)}{\left(R_r^2 + \left(L_rL_s - L_m^2\right)\omega_2/L_s - a_2^2\omega_v^2\right)^2 + \left(2a_2R_r\omega_v\right)^2}K_{pc1}U_0 - \frac{2a_2R_r^2\omega_v}{\left(R_r^2 + \left(L_rL_s - L_m^2\right)\omega_2/L_s - a_2^2\omega_v^2\right)^2 + \left(2a_2R_r\omega_v\right)^2} \times \left(K_{pc2}a_2\omega_v^2L_s/\left(L_rL_s - L_m^2\right) + K_{pc2}\omega_v\right)U_0.$$

In (30), the term containing K_{pc1} is the variation of rotor current generated by potential energy compensation branch. Since $a_2<0$, $A<0$, and $B<0$, *d*axis and *q*-axis increments of rotor current generated by potential energy compensation branch are both negative, i.e., it can to some degree decrease the rotor current during LVRT. However, since the oscillation frequency of stator voltage generated during LVRT ω_p is relatively small, and the value of oscillation frequency ω_v is much larger than the values of PI parameters in *dq* coordinate system, according to (30), the values of $A_{(1)}$ and $B_{(1)}$ are relatively small and scarcely affected by the parameters of energy compensation branch. Therefore, potential energy compensation branch has relatively small impact on LVRT capability of DFIG, scarcely changing the fundamental frequency characteristics of system.

The term containing K_{pc2} is the variation of rotor current generated by dissipation energy compensation branch. According to (30), affected by ω_v and a_2, both $A_{(2)}$ and $B_{(2)}$ are above 0, i.e., dissipation energy compensation branch will increase the rotor current during LVRT. As the parameters of dissipation energy compensation branch increase, the amplitude of rotor current will further increase, even reaching the limited value, making it difficult for rotor converter to operate normally and finally causing the system to go unstable.

Based on the abovementioned analysis, in excitation channel, the dissipation energy compensation branch will worsen LVRT performance of DFIG, thus, only potential energy compensation is applied, as shown in the red line in Fig. 5. While energy compensation branch in grid-side channel will not change the value of rotor current during LVRT, thus, dissipation energy compensation is applied to grid-side channel, as shown in Fig. 6.

D. Effect of Energy Remodeling in Multiple Frequency Bands and Parameter Optimization

The proposed energy compensation branches can adapt to the variation of oscillation frequency and realize dissipation energy and potential energy compensation in full frequency band, with different compensation effects in different frequency bands. To meet the requirement on system stability in sub/supersynchronous frequency bands, a scheme to optimize the parameters of energy compensation branches in multiple frequency bands is put forward.

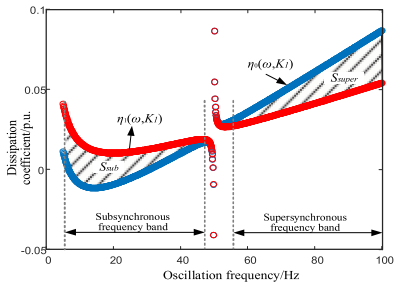

Fig. 7. Sub/supersynchronous frequency stability coefficient ratio.

First, the objective of parameter optimization is established. Define sub/supersynchronous frequency stability coefficient ratioσ as an index to evaluate the compatibility of energy compensation branch with the stability in supersynchronous frequency band, the expression of which is shown in (31). The bigger σ is, the smaller their impact on the stability in supersynchronous frequency band is, when improving the stability of system in subsynchronous frequency band

$$\begin{aligned} \sigma &= \left| \frac{S_{\text{sub}}}{S_{\text{super}}} \right| \\ S_{\text{sub}}(K) &= \int_{\omega_1}^{\omega_{1+}} \mu_1(\omega, K)\, d\omega - \int_{\omega_1}^{\omega_{1+}} \mu_0(\omega, K)\, d\omega \\ S_{\text{super}}(K) &= \int_{\omega_2}^{\omega_{2+}} \mu_1(\omega, K)\, d\omega - \int_{\omega_2}^{\omega_{2+}} \mu_0(\omega, K)\, d\omega \end{aligned} \tag{31}$$

where $S_{\text{super}/\text{sub}}(K)$ characterizes the effect of energy compensation branch on system stability coefficient in sub/supersynchronous frequency band, as shown in Fig. 7. Consider that the dangerous frequency bands where sub/supersynchronous oscillation may occur due to the introduction of series compensation line to DFIG are 5 Hz–30 Hz and 70 Hz–95 Hz [22], $2\pi 5 - 2\pi 30$ is chosen as the integration interval of $S_{\text{sub}}(K)$, and$2\pi 70 - 2\pi 95$ is chosen as the integration interval of $S_{\text{super}}(K)$.

Furthermore, according to requirements on stability of potential energy coefficient and dissipation energy coefficient in full frequency band, the constraints of parameters of energy compensation branches can be determined.

According to the minimum potential energy theorem [23], the system can only be stable at the point where the potential energy is the minimum. When $\xi(\omega,K) > 0$, the potential energy has a minimum value, thus, the system has stable equilibrium point. When $\xi(\omega,K) < 0$, the potential energy only has a maximum value, i.e., after the system is disturbed, it will gradually increase and cannot converge to stable state. Therefore, to guarantee that the system has stable equilibrium points in full frequency band, system potential energy coefficient, after energy compensation branches are added, should satisfy: $\min_{5\le\omega\le95} \xi(\omega, K) > 0$.

Dissipation energy coefficient can reflect the ability of system to dissipate oscillation. When $\eta(\omega,K) > 0$, the system has positive dissipation effect on oscillation, and the bigger $\eta(\omega,K)$ is, the better the dissipation effect is, the fast system oscillation converges. When $\eta(\omega,K) < 0$, the system has negative dissipation effect on oscillation, i.e., the dissipation energy will aggravate the diverging of system oscillation and cause the system to go unstable. Therefore, in order to meet the requirement on the dissipation effect in full frequency band, system dissipation energy coefficient should satisfy: $\min_{5\le\omega\le95} \eta(\omega, K) > 0$.

According to the abovementioned objective function and parameter constraints, a model to optimize the parameters of energy compensation branches in multiple frequency bands is constructed, shown in

$$\begin{aligned} &\max\ \sigma = \left| \frac{S_{\text{sub}}}{S_{\text{super}}} \right| \\ &\text{s.t.} \begin{cases} \min\limits_{5\le\omega\le95} \eta(\omega, K) > 0 \\ \min\limits_{5\le\omega\le95} \xi(\omega, K) > 0. \end{cases} \end{aligned} \tag{32}$$

Concerning the abovementioned model, the stochastic gradient method is used to determine the parameters of each energy compensation branch in the following steps.

Step 1: Apply DFIG control parameters to (23) and (27), and according to the constraints of dissipation energy coefficient and potential energy coefficient in (32), calculate the parameter boundary of energy compensation branch, which meets the requirement on system sub/supersynchronous stability in full frequency band, i.e., determine the search range of parameters.

Step 2: Set the initial values of parameters of energy compensation branch $K_{pc1(0)}$ and $K_{pc2(0)}$. According to the stochastic gradient method, update parameters $K_{pc1(1)}$ and $K_{pc2(1)}$ in the direction of negative gradient. If certain group of parameters satisfies the constraints in (32), this group of parameters is a feasible solution. If certain group of parameters does not satisfy the constraints, then regulate the step of negative gradient and do the "search and update" again until any feasible solution is found.

Step 3: Calculate sub/supersynchronous frequency stability coefficient ratio $\sigma_{(i)}$ corresponding to parameters $K_{pc1(\mathrm{i})}$ and $K_{pc2(\mathrm{i})}$. If $\sigma_{(i+1)} > \sigma_{(i)}$, $K_{pc1(\mathrm{i+1})}$, and $K_{pc2(\mathrm{i+1})}$ is the current optimal solution; otherwise, repeat Step 2.

Step 4: Repeat the search process until the number of iterations is satisfied. The current optimal solution is the optimal parameters of energy compensation branch.

After parameter optimization, the designed energy compensation branches are introduced in DFIG converter control system. The measurement of stator voltage is taken as the final input of energy compensation branches to realized active damping of subsynchronous oscillation.

It should be noted that, the proposed energy compensation branches are newly introduced control branches in DFIG converter control system, which do not affect parameters of the original control branches.

V. Simulation Verification

A. Test System

To verify the feasibility of the proposed method in real system, a simulation model is built in RT-LAB referring to the network

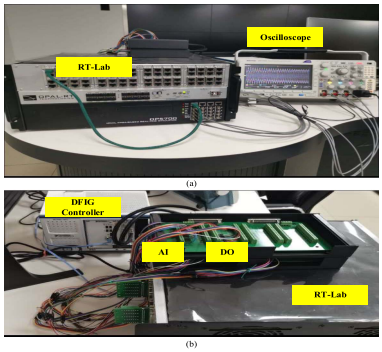

Fig. 8. Experimental platform. (a) RT-Lab and oscilloscope. (b) Connection between RT-Lab and DFIG controller.

TABLE II
DFIG PARAMETER SETTING

Parameter	Value	Parameter	Value
Rated power	1.5MW	Rotor resistance R_r	0.05631pu
Rated frequency	50Hz	Stator leakage inductance L_s	0.1pu
Stator rated voltage	0.69kV	Rotor leakage inductance L_r	0.03129pu
Stator resistance R_s	0pu	Mutual inductance L_m	0.13129pu
Integral gain of active power outer loop K_{i1}	20pu	Proportional gain of reactive power outer loop K_{p1}	0.05pu
Integral gain of reactive power outer loop K_{i2}	20pu	Proportional gain of active power outer loop K_{p2}	0.05pu
Integral gain of current inner loop K_{i3}	0.92pu	Proportional gain of current inner loop K_{p3}	0.0048pu
Integral gain of PLL $K_{i\ PLL}$	38.2pu	Proportional gain of PLL $K_{p\ PLL}$	3pu

topology and parameters of a real wind farm transmitted via the series C compensation system, shown in Fig. 8, where DFIG controller is an external physical controller containing DFIG rotor-side and grid-side converters, which generates converter control signals as input signals to RT-LAB for simulation analysis

DFIG parameter setting is shown in Table II. The control parameters used in the simulation tests in this article are all typical DFIG converter control parameters provided by the manufacturer. First, the variation of dissipation energy and potential energy coefficient as the oscillation frequency and parameters of energy compensation branches vary is calculated. And then, according to the proposed parameter optimization scheme, the optimal parameters of energy compensation branches are determined. Finally, through hardware-in-loop simulation tests, the effectiveness of the proposed control strategy in different oscillation cases and its compatibility with DFIG fundamental frequency characteristics are verified.

1) Optimization and Remodeling of Multiple Energy Branches

1) Remodeling of Excitation Channel Energy: After energy compensation is added to excitation voltage energy branch, the variation of system potential energy coefficient and dissipation energy coefficient are shown in Fig. 9. The variation of system potential energy coefficient is shown in Fig. 9(a). It can be seen that the remodeled excitation voltage energy branch has obvious compensation effect in subsynchronous frequency band. System potential energy coefficient gradually decreases as K_{pc1}

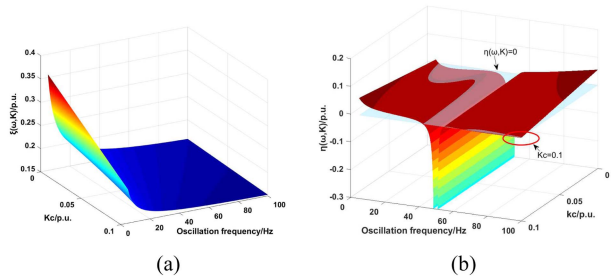

Fig. 9. Variation of system potential energy coefficient and dissipation energy coefficient as oscillation frequency and parameter of energy compensation branch vary after excitation voltage energy branch is remodeled.

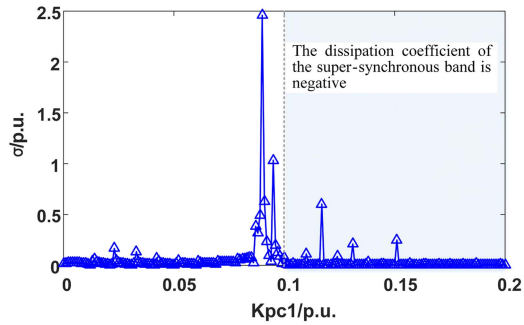

Fig. 10. Variation of sub/supersynchronous frequency stability coefficient ratio as parameter of excitation voltage energy compensation branch varies.

increases, and the stability of system gradually improves. In supersynchronous frequency band, the compensation effect of it is relatively small, but system potential energy coefficient still gradually decreases as K_{pc1} increase. Therefore, excitation voltage energy compensation branch can decrease the energy accumulated during oscillation and accelerate the converging of system oscillation.

The variation of system dissipation energy coefficient after excitation voltage energy compensation branch is introduced is shown in Fig. 9(b). It can be seen that, the added energy compensation branch can increase system dissipation energy coefficient in subsynchronous frequency band. However, in supersynchronous frequency band, system dissipation energy coefficient decreases due to negative compensation effect on dissipation energy. Thus, when setting the parameter of it, the requirement on dissipation energy in supersynchronous frequency band should be considered.

Furthermore, according to (32), parameter optimization model of excitation voltage energy compensation branch in multiple frequency bands is built, and the optimal parameter K_{pc1} is determined using the stochastic gradient method. According to the constraints of dissipation energy coefficient in supersynchronous frequency band, calculate the parameter boundary corresponding to $\min_{70\le\omega\le95}\eta(\omega,K)=0$, so that the value of K_{pc1} can be determined to be between 0 and 0.1 p.u. The optimization of K_{pc1} is shown in Fig. 10. It can be seen that, when K_{pc1} gradually increases from 0.01 p.u., σ also increases. When K_{pc1} reaches 0.09 p.u.,σ reaches the maximum value. At this time, the impact of excitation voltage energy compensation

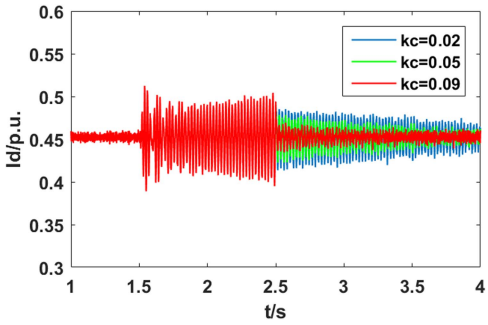

Fig. 11. Simulation results of excitation voltage energy compensation branch.

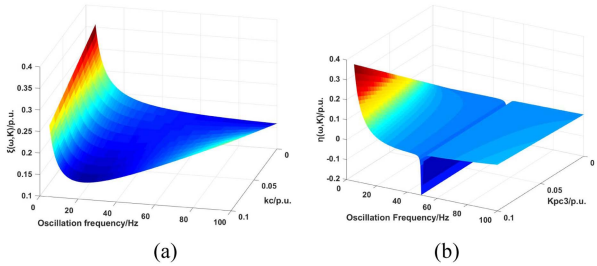

Fig. 12. Variation of system potential energy coefficient and dissipation energy coefficient as the oscillation frequency and parameter of energy compensation branch vary after grid-side energy branch is remodeled.

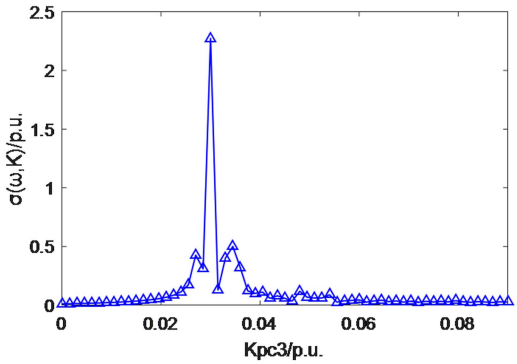

Fig. 13. Variation of sub/supersynchronous frequency stability coefficient ratio as the parameter of grid-side energy compensation branch varies.

branch on the stability of system in supersynchronous frequency band is the minimum. When K_{pc1} goes past 0.09 p.u., the compensation effect of excitation voltage energy compensation branch on dissipation energy in supersynchronous frequency band gradually becomes prominent, and σ in supersynchronous frequency band drops acutely. Therefore, the optimal parameter of excitation voltage energy compensation branch is determined to be 0.09 p.u.

To verify the effectiveness of excitation voltage energy compensation branch designed previously, hardware-in-the-loop simulations tests are conducted corresponding to $K_{pc1} = 0.02$, 0.05, and 0.09 p.u., respectively. Suppose series compensation line is switched ON at $t = 1.5$ s, which excites subsynchronous oscillation in the system, and excitation voltage energy compensation branch is switched ON at $t = 2.5$ s. The simulation results are shown in Fig. 11.

It can be seen from Fig. 11 that, subsynchronous oscillation excited by the series compensation system exhibits diverging trend. Without control, the system will gradually go unstable. After excitation voltage energy compensation branch is switched ON at $t = 2.5$ s, since the accumulated potential energy of system is offset by the energy compensation branch, the oscillation amplitude drops. And, the bigger parameter K_{pc1} is, the more obvious the compensation effect on potential energy is. When $K_{pc1} = 0.09$ p.u., the oscillation amplitude drops to 1/5 of the original value. Meanwhile, since the accumulated potential energy decreases, the dissipation intensity of system can meet the requirement on energy dissipation during oscillation. It can be seen that, the oscillation converges faster and reaches stable state in 0.5 s, thus, the stability of sub/super-synchronous oscillation is greatly improved.

2) Remodeling of Grid-Side Channel Energy: After energy compensation branch is added to grid-side channel, the variation curves of system potential energy and dissipation energy coefficient as the oscillation frequency and parameter of energy compensation branch vary are shown in Fig. 12.

Fig. 12(a) depicts the variation of system potential energy coefficient. It can be seen that, in subsynchronous frequency band, grid-side energy compensation branch can reduce the potential energy coefficient and improve system stability. However, in supersynchronous frequency band, it will increase the potential energy coefficient. Besides, as K_{pc3} increases, its potential energy compensation effect also gradually increases, which will lower the stability of system in supersynchronous frequency band. Therefore, when setting the parameter of the branch, the requirement on potential energy in supersynchronous frequency band should be considered.

The variation of system dissipation energy coefficient is shown in Fig. 12(b). It can be seen that grid-side energy compensation branch obviously increases system dissipation energy coefficient in subsynchronous frequency band, thus accelerating the converging of subsynchronous oscillation. In supersynchronous frequency band, the positive dissipation compensation effect of grid-side energy compensation branch is relatively small. However, as K_{pc3} increases, it still exhibits positive dissipation compensation effect, improving the stability of system in supersynchronous frequency band.

Furthermore, according to (32), parameter optimization model of grid-side energy compensation branch in multiple frequency bands is built, and its optimal parameter K_{pc3} is determined using the stochastic gradient method. The optimization of K_{pc3} is shown in Fig. 13. It can be seen that when $K_{\mathrm{pc3}} < 0.03$ p.u., as K_{pc3} increases, σ also gradually increases. When $K_{\mathrm{pc3}} = 0.03$ p.u., σ reaches the maximum value, when the impact of grid-side energy compensation branch on the stability level of system in supersynchronous frequency band is the minimum. When $K_{\mathrm{pc3}} > 0.03$ p.u., since potential energy coefficient in supersynchronous frequency band increases acutely as K_{pc3} increases, σ gradually drops. Therefore, the optimal parameter of grid-side energy compensation branch is determined to be $K_{pc3} = 0.03$ p.u.

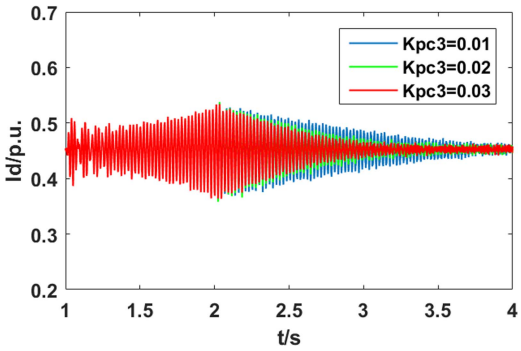

Fig. 14. Simulation results of grid-side energy compensation branch.

To verify the effectiveness of grid-side energy compensation branch designed previously, hardware-in-the-loop simulations tests are conducted corresponding to $K_{pc3} = 0.01$ p.u., 0.02 p.u., and 0.03 p.u., respectively. Suppose grid-side energy compensation branch is switched on at $t = 2$ s, and the variation curves of d-axis current are shown in Fig. 14.

It can be seen from Fig. 14 that, at the instant when the grid-side energy compensation branch is switched ON, system oscillation amplitude scarcely changes. This is because, the potential energy compensation term in the grid-side energy compensation branch is relatively small, thus, it does not affect the accumulation of potential energy during oscillation. However, since the dissipation energy compensation effect of it is relatively big, system dissipation intensity obviously increases at the instant, and the oscillation of d-axis current turns from diverging to converging. As K_{pc3} increases, the dissipation energy compensation effect is more obvious, and the converging of oscillation also gradually speeds up.

Furthermore, according to Figs. 9 and 12, after the parameters optimization, the potential energy and dissipation energy generated by excitation voltage and grid-side voltage energy compensation branches in supersynchronous frequency band can compensate for each other. That is to say, the negative dissipation energy compensation caused by excitation voltage compensation branch in supersynchronous frequency band can be offset by the positive dissipation compensation caused by the grid-side voltage compensation branch. Similarly, the negative potential compensation caused by excitation voltage compensation branch in supersynchronous frequency band can offset the positive potential compensation caused by the grid-side voltage compensation branch. Therefore, when both the excitation voltage and grid-side voltage energy compensation branches are added, the proposed control strategy can satisfy the stability requirement of supersynchronous frequency band and effectively suppress system oscillation in super-synchronous frequency band.

C. Verification of the Adaptability to Different Oscillation Cases of the Proposed Control Strategy

To verify the contribution of the proposed method in adaptability to different oscillation cases, the value of the capacitance of the series compensation line is adjusted to excite different oscillation cases for simulation. The comparison between the proposed control strategy and commonly used rotor current compensation control [13] is also made for validation.

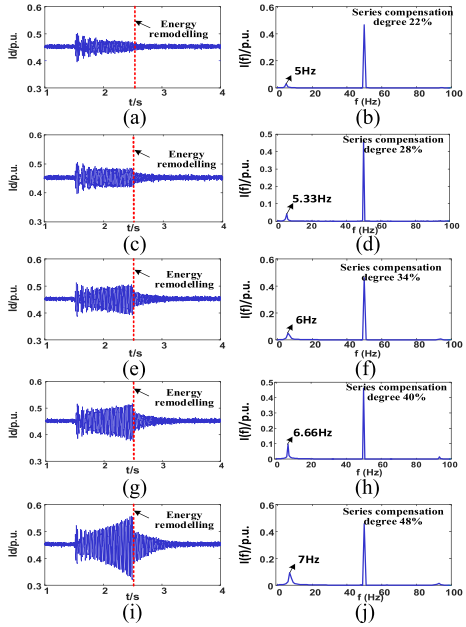

Fig. 15. Active damping control effects corresponding to different series compensation degrees.

Suppose series compensation line is switched ON at $t = 1.5$ s with the series compensation degree being 22%, 28%, 34%, 40%, and 43%. The frequencies of subsynchronous oscillation excited in DFIG-integrated power system are, respectively, 5, 5.33, 6, 6.66, and 7 Hz. In the abovementioned five oscillation cases, excitation voltage and grid-side energy compensation branches are both switched ON at $t = 2.5$ s. Simulation results of the proposed control strategy are shown in Fig. 15.

It can be seen from Fig. 15(a) and (b) that, when series compensation degree is 22%, the subsynchronous oscillation excited in the system converges slowly. After energy compensation branch is switched ON at $t = 2.5$ s, the oscillation converges faster and the system reaches stable state at $t = 2.6$ s.

When series compensation degree increases to 28%, the oscillation curve of d-axis current and the oscillation spectrum of grid-side current are shown in Fig. 15(c) and (d). It can be seen that constant-amplitude subsynchronous oscillation is excited in the system. After energy compensation branch is switched ON, the oscillation amplitude of d-axis current immediately drops due to potential energy compensation effect. At the same time, since dissipation energy coefficient increases, system oscillation gradually turns to stable state.

When series compensation degree increases from 34% to 48%, diverging oscillation is excited in the system with the oscillation frequency being 6–7 Hz, and in these cases the oscillation curves of d-axis current and the oscillation spectrums of grid-side current are shown in Fig. 15(e)–(j). It can be seen that, as series compensation degree increases, the amplitude of system oscillation also increases, so does the diverging speed. After energy compensation branch is switched ON at $t = 2.5$ s,

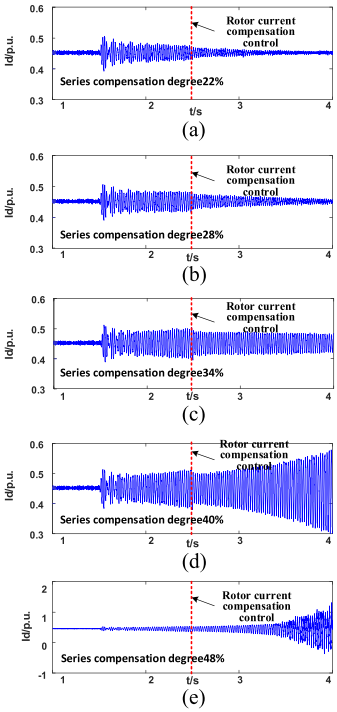

Fig. 16. Control effects of rotor current compensation method corresponding to different series compensation degrees.

since the compensation effect of energy compensation branch also increases as series compensation degree rises, in these cases the oscillation amplitude of d-axis current drops to below 1/2 of the original value and system oscillation converges to stable state in 0.5 s.

Simulation results of the rotor current compensation method are shown in Fig. 16, where it can be seen that, when the series compensation degree is 22% and 28%, system oscillation has constant amplitude, and rotor current compensation method can damp the oscillation. When the series compensation degree increases to 34%, the damping effect of the method obviously drops, and system oscillation converges slowly. When the series compensation degree increases to 48%, it can no longer meet the damping demand of system, and the oscillation gradually diverges. This is because, rotor current compensation method adds fixed damping compensation in RSC, which does not vary as the oscillation scene varies. Thus, when the series compensation degree further increases, the method may fail to meet the damping demand. Comparison between Figs. 15 and 16 show the proposed control strategy can adapt to different oscillation cases.

D. Verification of the Compatibility With Supersynchronous Frequency Band of the Proposed Control Strategy

To verify the contribution of the proposed method in compatibility with supersynchronous frequency band, forced oscillation caused by the injection of external harmonic source is taken for simulation. The comparison between the proposed control strategy and rotor current compensation control is also made for validation.

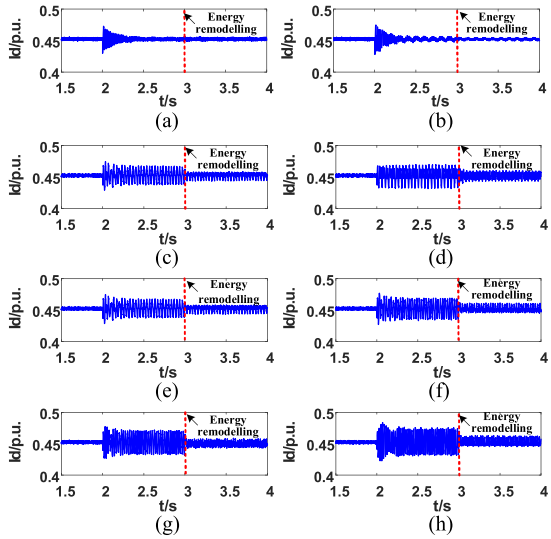

Fig. 17. Active damping control effects corresponding to harmonic sources with different oscillation frequencies.

Suppose harmonic voltage source with the oscillation frequency being 60–95 Hz is switched on in DFIG-integrated power system at $t = 2$ s, and excitation voltage and grid-side energy compensation branches are both switched ON at $t = 3$ s. Simulation curves of the proposed method are shown in Fig. 17.

Fig. 17(a) shows the oscillation curve of DFIG d-axis current excited by 60 Hz harmonic voltage source. It can be seen that, a 10 Hz oscillation component is induced in d-axis current. However, since the slip of DFIG at such frequency is relatively small, the oscillation component induced in d-axis current is not obvious. When the oscillation frequency of harmonic source increases to 65 Hz, the oscillation curve of DFIG d-axis current is shown in Fig. 17(b). In this case, a 15 Hz oscillation component is induced in d-axis current. After energy compensation branch is switched ON, the oscillation component in d-axis current drops to 1/3 of the original value.

When the oscillation frequency of harmonic voltage source varies from 70 Hz to 95 Hz, the oscillation curve of d-axis current is shown in Fig. 17(c)–(h). It can be seen that, the higher the oscillation frequency is, the larger the oscillation amplitude is. After energy compensation branch is switched ON, since the energy compensation branch offsets the potential energy accumulated during oscillation, the oscillation amplitude of d-axis current obviously drops. The higher the oscillation frequency is, the bigger the potential energy compensation effect is, and in supersynchronous frequency band, the percentage of induced oscillation component in d-axis current drops from 20% to below 10%.

Simulation curves of rotor current compensation method are shown in Fig. 18. It can be seen that, in supersynchronous frequency band, the damping effect of the method is not obvious. Especially in the frequency band of 60–70 Hz, this control strategy has scarcely any damping effect on system oscillation. In the frequency band of 75–95 Hz, rotor current compensation method causes the amplitude of system oscillation to drop, but its damping effect is relatively weak compared with that of the

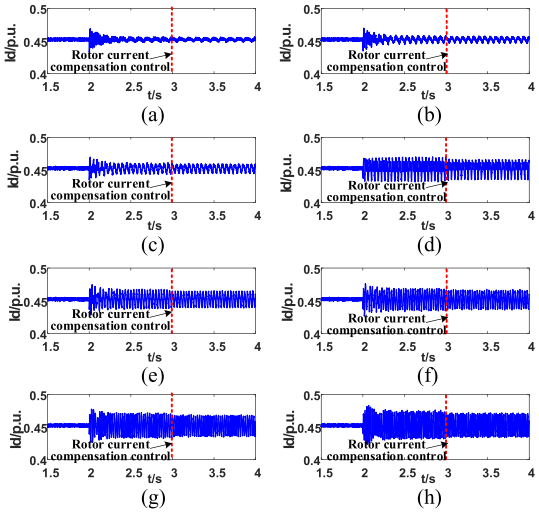

Fig. 18. Control effects of rotor current compensation method corresponding to harmonic sources with different oscillation frequencies.

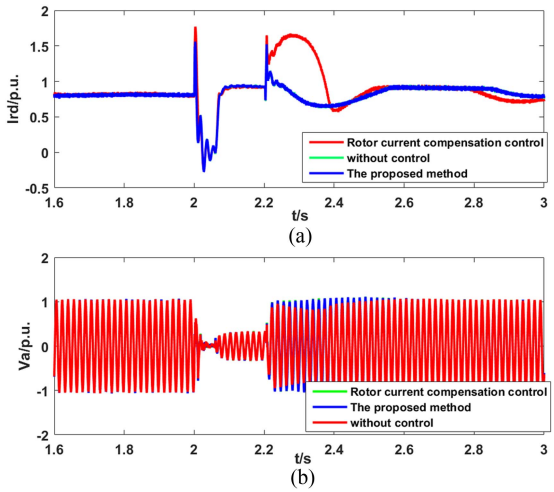

Fig. 19. Waveforms of DFIG terminal voltage and rotor current during LVRT with rotor current compensation, with the proposed energy branch compensation and without compensation control.

proposed method. This is because, the control parameters of the method are designed only for subsynchronous frequency band, and system stability in supersynchronous frequency band is not considered. Besides, rotor current compensation method only uses RSC to suppress oscillation without considering the damping effect of GSC, thus, its control effect is limited. The proposed method based on collaborative control of RSC and GSC can effectively improve the active damping effect of DFIG.

E. Verification of the Compatibility With Fundamental Frequency Characteristics of the Proposed Control Strategy

To verify the compatibility of the proposed energy compensation branches with DFIG fundamental frequency characteristics, the LVRT process of DFIG is simulated in this article by setting three-phase short circuit fault on the line via which DFIG is integrated to the grid. Suppose the fault lasts for 0.2 s and the fault resistance is 0.01Ω.

LVRT characteristics of DFIG with energy branch compensation and rotor current compensation are verified, the comparative simulation curves shown in Fig. 19.

Fig. 19(a) depicts the variation curves of DFIG rotor current during LVRT, where the variation curve of DFIG with rotor current compensation is shown in red. It can be seen that DFIG rotor current has sudden increase both at the instant of LVRT and in the voltage restoration process, with the overcurrent value reaching nearly three times the rated value. Thus, stable operation of rotor converter is endangered, as well as effective LVRT of DFIG. The variation curve of DFIG with the proposed energy branch compensation is shown in blue. It can be seen that, there is no obvious difference between DFIG rotor currents with energy branch compensation and without energy branch compensation. Thus, energy branch compensation does not affect DFIG induction current and electromotive force during LVRT, and normal operation of rotor converter can be guaranteed.

Fig. 19(b) depicts the variation curves of DFIG stator voltage during LVRT. It can be seen that, compared with DFIG without compensation control, the terminal voltage of DFIG with rotor current compensation control drops even more during LVRT and voltage restoration, which worsens the problem of LVRT. The proposed energy branch compensation scarcely affects the variation of DFIG stator voltage during LVRT. Therefore, the proposed method is compatible with fundamental frequency characteristics of DFIG.

VI. Conclusion

This article constructs potential energy and dissipation energy compensation branches in key energy branches of DFIG. The locations and parameters of energy compensation branches are optimized, considering the compatibility with DFIG fundamental frequency characteristics and the stability of system in sub/supersynchronous frequency bands. On this basis, an optimal remodeling of multiple energy branches in full frequency band is realized. The main conclusions are listed as follows.

1) Among the components of system dynamic energy, potential energy component, and dissipation energy component are key factors that characterize the stability level of system. According to Lyapunov's second law, the bigger dissipation energy is and the smaller potential energy is, the faster the potential energy accumulated during oscillation is consumed, i.e., the higher system stability level is.
2) Energy compensation branches constructed in this article are based on stator voltage components and can adapt to the variation of oscillation frequency and different oscillation cases when compensating for potential energy and dissipation energy, not limited to single resonance frequency point.
3) In parameter setting of energy compensation branches, the requirement of the stability in supersynchronous frequency band is considered. After the parameters optimization, the potential energy and dissipation energy generated by excitation voltage and grid-side voltage energy

compensation branches in supersynchronous frequency band can compensate for each other. Thus, the proposed control strategy can meet the stability requirement of supersynchronous frequency band, and effectively suppress system oscillation in supersynchronous frequency band.

4) The proposed active damping control strategy based on remodeling of multiple energy branches does not affect the dynamic characteristics of DFIG rotor current and terminal voltage during LVRT, thus, it is compatible with fundamental frequency characteristics of DFIG.

REFERENCES

[1] D. H. R. Suriyaarachchi, U. D. Annakkage, C. Karawita, and D. A. Jacobson, "A procedure to study sub-synchronous interactions in wind integrated power systems," *IEEE Trans. Power Syst.*, vol. 28, no. 1, pp. 377–384, Jul. 2012.

[2] R. K. Patnaik, P. K. Dash, and K. Mahapatra, "Adaptive terminal sliding mode power control of DFIG based wind energy conversion system for stability enhancement," *Int. Trans. Elect. Energy Syst.*, vol. 26, pp. 750–782, Jun. 2016.

[3] J. L. Domínguez-García, O. Gomis-Bellmunt, F. D. Bianchi, and A. Sumper, "Power oscillation damping supported by wind power: a review," *Renewable Sustain. Energy Rev.*, vol. 16, pp. 4994–5006, Sep. 2012.

[4] M. R. A. Pahlavani and H. A. Mohammadpour, "Damping of subsynchronous resonance and low-frequency power oscillation in a series-compensated transmission line using gate-controlled series capacitor," *Elect. Power Syst. Res.*, vol. 81, pp. 308–317, Feb. 2011.

[5] B. Gao and Y. Hu, ''Sub-synchronous resonance mitigation by a STATCOM in doubly fed induction generator-based wind farm connected to a series-compensated transmission network," *J. Eng.*, vol. 2019, no. 16, pp. 812–815, 2019.

[6] Moharana, R. K. Varma, and R. Seethapathy, "SSR Alleviation by STATCOM in induction-generator-based wind farm connected to series compensated line," *IEEE Trans. Sustain. Energy*, vol. 5, no. 3, pp. 947–957, Jul. 2014.

[7] H. Xie, B. Li, C. Heyman, M. M. de Oliveira, and M. Monge, "Subsynchronous resonance characteristics in presence of doubly-fed induction generator and series compensation and mitigation of subsynchronous resonance by proper control of series capacitor," *IET Renewable Power Gener.*, vol. 8, no. 4, pp. 411–421, May 2014.

[8] H. Liu, X. Xie, Y. Li, H. Liu, and Y. Hu, "Mitigation of SSR by embedding subsynchronous notch filters into DFIG converter controllers," *IET Gener. Transmiss. Distribution*, vol. 11, no. 11, pp. 2888–2896, Aug. 2017.

[9] A. K. Chen, D. Xie, D. Zhang, C. Gu, and K. Wang, "PI parameter tuning of converters for sub-synchronous interactions existing in Grid-connected DFIG wind turbines," *IEEE Trans. Power Electron.*, vol. 34, no. 7, pp. 6345–6355, Jul. 2019.

[10] L. Wang, X. Xie, Q. Jiang, H. Liu, Y. Li, and H. Liu, "Investigation of SSR in practical DFIG-based wind farms connected to a series compensated power system," *IEEE Trans. Power Syst.*, vol. 30, no. 5, pp. 2772–2779, Sep. 2015.

[11] G. D. Irwin, A. K. Jindal, and A. L. Isaacs, "Sub-synchronous control interactions between type 3 wind turbines and series compensated AC transmission systems," in *Proc. IEEE Power Energy Soc. Gen. Meet.*, Detroit, MI, USA, 2011, pp. 1–6.

[12] Y Song, X. Wang, and B. Frede,. "Doubly fed induction generator system resonance active damping through stator virtual impedance," *IEEE Trans. Ind. Electron.*, vol. 64, no. 1, pp. 125–137, Jan. 2017.

[13] W. Ning, X. Wu, Y. J. Guan, and F. Chen, "Method to suppress subsynchronous oscillation of DFIG-based wind farms based on virtual impedance," *J. Eng.*, vol. 2017, no. 13, pp. 2173–2177, 2017.

[14] J. Ma, Y. Shen, and A. G. Phadke, "Stability assessment of DFIG Subsynchronous oscillation based on energy dissipation intensity analysis," *IEEE Trans. Power Electron.*, vol. 35, no. 8, pp. 8074–8087, Aug. 2020.

[15] S. Thomsen, K. Rothenhagen, and F. W. Fuchs, "Online parameter identification methods for doubly fed induction generators," in *Proc. IEEE Power Electron. Specialists Conf.*, 2008, pp. 2735–2741.

[16] X. Pan, R. Wen, P. Ju, Y. Jin, and Y. Zhang. "A frequency-domain based method to identify parameters of grid side converter controller for doubly fed induction generators," *Power Syst. Technol.*, vol. 39, no. 3, pp. 634–638, 2015.

[17] V. Valdivia, A. Barrado, A. LÃzaro, P. Zumel, C. Raga, and C. FernÃndez, "Simple modeling and identification procedures for "Black-Box" behavioral modeling of power converters based on transient response analysis," *IEEE Trans. Power Electron.*, vol. 24, no. 12, pp. 2776–2790, Dec. 2009.

[18] Z. Miao, "Impedance-model-based SSR analysis for type 3 wind generator and series-compensated network," *IEEE Trans. Energy Convers.*, vol. 27, no. 4, pp. 984–991, Dec. 2012.

[19] M. Mohseni and S. M. Islam. "Review of international grid codes for wind power integration: Diversity, technology and a case for global standard," *Renewable Sustainable Energy Rev.*, vol. 6, no. 16, pp. 3876–3890, 2012.

[20] M. Tsili and S. Papathanassiou, "A review of grid code technical requirements for wind farms," *IET Renewable Power Gener.*, vol. 3, no. 3, pp. 308–310, Sep. 2009.

[21] C. Wessels, F. Gebhardt, and F. W. Fuchs, "Fault ride-through of a DFIG wind turbine using a dynamic voltage restorer during symmetrical and asymmetrical Grid faults," *IEEE Trans. Power Electron.*, vol. 26, no. 3, pp. 807–815, Mar. 2011.

[22] X. Xie, X. Zhang, H. Liu, H. Liu, Y. Li, and C. Zhang, "Characteristic Analysis of subsynchronous resonance in practical wind farms connected to series-compensated transmissions," *IEEE Trans. Energy Convers.*, vol. 32, no. 3, pp. 1117–1126, Sep. 2017.

[23] D. G. Pavlou, *The Principle of Minimum Potential Energy for One-Dimensional Elements*. Cambridge, MA, USA: Academic, 2015, pp. 279–288.

Jing Ma (Senior Member, IEEE) received the B.S. and Ph.D. degrees from North China Electric Power University, Beijing, China, in 2003 and 2008, respectively.

He was a Visiting Research Scholar with the Bradley Department of Electrical and Computer Engineering, Virginia Polytechnic Institute and State University, from 2008 to 2009. He is currently a Professor with the School of Electrical and Electronic Engineering, North China Electric Power University, China. His research interests include power system stability and control.

Yaqi Shen was born in Jiangsu Province, China. She is currently working toward the Ph.D. degree with the School of Electrical and Electronic Engineering, North China Electric Power University, Beijing, China.

Her research interests include power system stability analysis and control.